

A Genealogy of Foundation Models in Remote Sensing

KEVIN LANE and MORTEZA KARIMZADEH, University of Colorado, Boulder, USA

Foundation models have garnered increasing attention for representation learning in remote sensing. Many such foundation models adopt approaches that have demonstrated success in computer vision with minimal domain-specific modification. However, the development and application of foundation models in this field are still burgeoning, as there are a variety of competing approaches for how to most effectively leverage remotely sensed data. This paper examines these approaches, along with their roots in the computer vision field. This is done to characterize potential advantages and pitfalls, while outlining future directions to further improve remote sensing-specific foundation models. We discuss the quality of the learned representations and methods to alleviate the need for massive compute resources. We first examine single-sensor remote foundation models to introduce concepts and provide context, and then place emphasis on incorporating the multi-sensor aspect of Earth observations into foundation models. In particular, we explore the extent to which existing approaches leverage multiple sensors in training foundation models in relation to multi-modal foundation models. Finally, we identify opportunities for further harnessing the vast amounts of unlabeled, seasonal, and multi-sensor remote sensing observations.

CCS Concepts: • General and reference → Surveys and overviews; • Computing methodologies → Image representations; Reconstruction; • Applied computing → Environmental sciences; • Information systems → Spatial-temporal systems.

Additional Key Words and Phrases: Foundation Models, Remote Sensing, Self-Supervised Learning

ACM Reference Format:

Kevin Lane and Morteza Karimzadeh. 2025. A Genealogy of Foundation Models in Remote Sensing. 1, 1 (November 2025), 35 pages. <https://doi.org/10.1145/nnnnnnn.nnnnnnn>

1 Introduction

With the recent successes of Natural Language Processing (NLP) frameworks like Generative Pre-trained Transformers (GPT) [92] and Bi-directional Encoder Representations from Transformers (BERT) [36], the development and application of machine learning is shifting away from focusing on transfer learning. Transfer learning uses traditional supervised learning on a large, labeled dataset to learn representations of that data to apply to other related tasks. Instead, Self-Supervised Learning (SSL), which learns general-purpose representations of data without the need for external labels, has risen in popularity [25]. As datasets have grown larger, with some datasets now containing billions of data points [35], the process of labeling data for supervised learning has proven to be a costly bottleneck for improving model performance. SSL circumvents this issue with the use of pretext tasks: auxiliary learning objectives designed to leverage the natural structure of unlabeled data in order to learn patterns or relationships within the data. Researchers can then fine-tune these pre-trained models for specific downstream tasks on significantly smaller labeled datasets. Fine-tuning enables downstream users to achieve state-of-the-art (SOTA) performance on a specific task while incurring significantly

Authors' Contact Information: Kevin Lane, kevin.lane@colorado.edu; Morteza Karimzadeh, karimzadeh@colorado.edu, University of Colorado, Boulder, Colorado, USA.

Permission to make digital or hard copies of all or part of this work for personal or classroom use is granted without fee provided that copies are not made or distributed for profit or commercial advantage and that copies bear this notice and the full citation on the first page. Copyrights for components of this work owned by others than the author(s) must be honored. Abstracting with credit is permitted. To copy otherwise, or republish, to post on servers or to redistribute to lists, requires prior specific permission and/or a fee. Request permissions from permissions@acm.org.

© 2025 Copyright held by the owner/author(s). Publication rights licensed to ACM.

Manuscript submitted to ACM

lower costs than training an equivalent model from scratch [3]. Thus, effective SSL training democratizes access to high performance machine learning models.

In the wake of NLP success, the computer vision (CV) field swiftly delved into SSL with foundation models such as BYOL [46], SimCLR [23], MoCo [50], and DINO [18], all of which use unique approaches to create self-supervised tasks and objectives for natural imagery data. These methodologies have recently started to percolate into the field of remote sensing (RS), where the sheer amount of unlabeled data from satellite imagery makes the field ripe for the development of foundation models. Satellite imagery can be used for environmental monitoring tasks, such as monitoring or forecasting wildfires. Climate change's impact on such events means that there is imminent use for these generalized representations for downstream tasks.

Thus far, the self-supervised methods for foundation models in RS build heavily upon CV methods and fall broadly into one of four categories:

- (1) Contrastive learning via negative sampling
- (2) Contrastive learning via distillation
- (3) Contrastive learning via redundancy reduction
- (4) Masked image modeling

Most of these approaches have demonstrated significant promise in the RS domain but have largely remained limited to applying the same CV frameworks to satellite imagery and other remote sensing datasets with few to no methodology changes [101]. However, recent research demonstrates how satellite data has unique properties that are distinct from natural imagery, such as the logarithmic distribution of objects and the range of the electromagnetic spectrum captured within satellite images [101]. These properties indicate that satellite imagery is a distinct modality and would therefore benefit from modality-specific frameworks and self-supervised learning tasks. Moreover, the variety of different satellite and ground-level sensors available allows for the development of highly specialized multi-modal foundation models. In this paper, we contribute to the growing body of research on foundation models in remote sensing by doing the following:

- (1) We further demonstrate how the modes of data available in RS provide unique information that sets them apart from the natural imagery of CV.
- (2) We survey recent foundation models developed in the field, categorized by their learning objective, and discuss their specific adaptations for RS observations.
- (3) We identify gaps and outline research opportunities for RS foundation models. We specifically consider the multi-sensor and multi-modal nature of RS observations, and how to effectively leverage such data at scale.

2 Prior Work

Recent papers in the field have surveyed available foundation models in RS. Zhou explored the high potential of applied Vision Language Models (VLMS) while highlighting their few shot capabilities in downstream tasks [141]. Chen inspected how models can adapt to utilize non-raster based data [25], such as poly-lines, to represent transportation networks. Zhang examined the singular task of building foundation models specifically for urban environments [138]. Mai created a 'wish list' of desirable traits in RS foundation models, with rationale for each wish, and discussed where current foundation models exceed or fall short of these goals [82]. Lu categorized the model backbones, training datasets, image resolution, and over-arching pre-training methods for existing RS foundation models [80]. Lu also documented the number of parameters for each model and compiled results across a wide range of diverse downstream tasks [80].

While these works provide a timely review of important components in RS foundation models, none of them focus on the specific adaptations that have been made to SSL approaches for working with remote sensing data. Works such as [143] might note that ideal RS foundation models should factor in temporal features, but do not spend time exploring the ins-and-outs of how current models do so. Surveys such as [80] comprehensively document the different datasets, backbones, and broad SSL tasks used by RS foundation models. However, they do not delineate the differences in models past this point, preferring to focus instead on model performance. While comprehensive benchmarking is helpful, differences in models' learning objectives such as the use of temporally positive pairs, adaptation to multi-scale view, or leveraging a remote sensing index as a reconstruction target, are all glossed over. These kinds of adaptations for RS data inform model performance and effective downstream use, and more importantly, future research directions. We fill that gap here by discussing these unique adaptations.

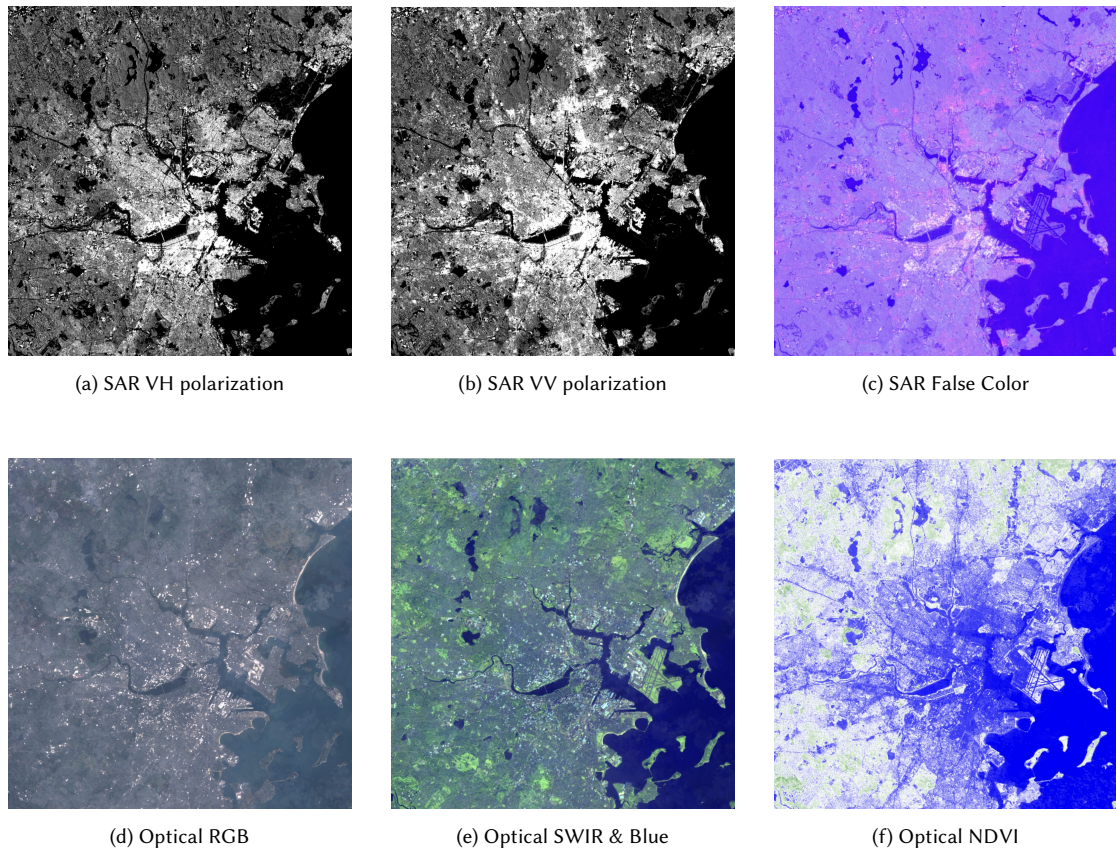


Fig. 1. Satellite imagery of Boston, MA in October, 2020. SAR imagery is obtained from Sentinel-1, and optical imagery is obtained from Sentinel-2. SAR false color uses VV polarization for red channel, VH polarization for green channel, and the average of VV and VH polarizations for blue channel. NDVI refers to the Normalized Difference Vegetation Index, an index based on the Red and Near Infrared (NIR) bands that is utilized to assess vegetation health.

3 Data for Training Remote Sensing Foundation Models

The CV field has primarily been concerned with natural images, which only sense the red, green, and blue wavelengths of the visible spectrum, and are typically captured at ground level. Some models, such as CLIP [98], FLIP [63], VisualBERT [72], ViLBERT [79], FLAVA [106], and DeepSeek-VL2 [129] are VLMs that also utilize text as an additional mode of data. However, most of the RS foundation model frameworks borrowed from CV concern themselves with only the image modality. Within the RS domain, the variety of unique sensors available ranges across a number of instruments aboard different satellites. The data modes detailed below are available at mass scale and readily accessible for training foundation models. The training of RS foundation models is our focus in this manuscript, rather than providing a full catalogue of remote sensing or geospatial data. We will keep discussions focused on sensors with high resolution (e.g., less than 40m), which are also the focus of current efforts in benchmarking datasets [71] and training foundation models [141].

3.1 Optical Imagery

Optical images capture electromagnetic wavelengths in the visible and near visible bands of light. These are recorded via passive sensors, which simply measure the electromagnetic radiation originating from the sun that is reflected off of objects. This means that passive sensors are more energy efficient than active sensors, but they are affected by light and weather conditions. These sensors can only capture imagery during the daytime, and can be obscured by atmospheric phenomena like cloud cover or haze. This means their use is limited in hurricanes, storms or active floods under overcast conditions.

Optical images are often acquired from different satellites. Several datasets from different satellites are openly available for free, mass download, such as MODIS [65], the Landsat [130] family, and Sentinel-2 [110], with the latter two offering high resolution. Each satellite contains a sensor with different spatial and spectral resolutions, but each is broadly designed to capture the visible, near-infrared, and short-wave infrared portions of the electromagnetic spectrum. In the case of the Sentinel-2 satellite, there are 13 distinct bands that are captured at resolutions ranging from 10m/pixel to 60m/pixel. These bands can be broken down into five groups based on usage as follows [122]:

- B1 is the coastal aerosol band, useful for mapping coastal marine habitats and bathymetry. [96]
- B2-4 capture RGB (Red Green Blue), similar to digital cameras.
- B5-8 refer to VNIR (Visible and Near Infrared) light, and are typically used to measure vegetation health. B8a is a Narrow Near Infrared (NIR) band for moisture-based vegetation health monitoring.
- B9, still in NIR spectrum, focuses on water vapor absorption and is used to measure atmospheric moisture presence. It is paired with B8A to derive total precipitable water.
- B10-B11 are SWIR (Short Wave Infrared) bands. B10 is used for cirrus cloud detection. B11 is used for soil and vegetation moisture detection and snow/ice vs. cloud differentiation. B12 is often used with B2 to measure geological features and map burned areas.

This range of spectrum and information captured by Sentinel-2 is an example of the wealth of information captured by remote sensing optical products that go beyond RGB. However, CV models are designed to operate with three input channels of RGB of ‘natural’ images (obtained by regular cameras and widely available on the internet). In order to leverage the highly sophisticated pre-trained weights that are available for CV backbones, such as the ubiquitous ResNet50 [51] or ViT16 [37], some RS models only utilize the visible bands of light from optical multispectral (MS) satellite images [26, 84]. Some RS models also rely on RGB images taken at ground level [20], or from some sort of aerial

platform, such as a drone or helicopter [75]. While RS models trained purely on RGB can achieve SOTA performance in certain settings [84], deep learning models in RS that only train on RGB data have an information disadvantage compared to models that train on all bands. RGB-only models can struggle to perform on a number of downstream tasks in RS as a result [71]. The spectral range of interest and the specific choice of bands on a satellite are the result of decades of experience, in-lab experiments and consensus-building efforts to ensure satellites are equipped with bands that can assist in target-specific tasks. Figure 1 highlights the information lost when solely examining RGB imagery. For instance, infrared bands are crucial for monitoring vegetation [90], as seen in figure 1f, while NIR bands in confluence with blue and green bands can help with water quality analysis [30]. SWIR can be used for measuring soil and vegetation moisture, and is depicted in figure 1e.

While an increasing number of foundation models leverage most bands present in optical imagery such as Sentinel-2, they typically do so by a simple manipulation of input channel dimensions to the image encoder of the model [124]. The optimal architecture required for remote sensing architectures is not well-defined yet [101].

3.2 Synthetic Aperture Radar

Synthetic Aperture Radar (SAR) is an active remote sensor that emits energy in microwave frequencies towards the earth and then captures the amount of energy reflected back. Capturing the image from a moving sensor (in this case, a satellite) allows for capturing the image through a large 'synthetic' aperture, compared to the much smaller physical sensor aperture. This results in a much higher resolution than other sensors that monitor similar frequencies [15]. Each SAR sensor operates in a specific wavelength, referred to as bands, which serve different uses [119]. Larger wavelengths provide more penetration through obstruction, such as vegetation, but result in lower resolution. One of the most commonly used bands is C-band (7.5-3.8 cm wavelength) [119], which is currently captured by Sentinel-1 [117], RADARSAT-1 [81], RADARSAT-2 [87], RADARSAT Constellation Mission (RCM) [116] satellites. C-band imagery is made available publicly, and is useful for global mapping and change detection. The larger wavelength provides moderate penetration still at relatively high spatial resolution (e.g., 40m). However, there are larger wavelengths available, such as L-band, which is captured by AirSAR [53], PALSAR [103], and the soon-to-be-launched NISAR [21]. L-band is often used for biomass and vegetation mapping [48]. There is also X-band, whose wavelength is smaller than C-band and often used for high resolution monitoring of fine surface features, such as vegetation structure, and urban infrastructure. [108]. X-band is obtained by platforms such as Capella [19], ICEYE [57], TerraSAR-X [128], and TanDEM-X [70]. Different wavelengths of SAR all capture different information, and different wavelengths often complement each other if available for the same region and time.

SAR has another characteristic distinct from optical imagery: SAR takes advantage of materials' innate dielectric properties. Every material has a dielectric constant that describes how strongly it interacts with electromagnetic waves. Materials with a high dielectric constant, such as water, reflect microwave energy back more strongly, allowing it to be picked up more easily by SAR [11]. This can prove useful for applications such as mapping waterways in a region that might be otherwise undetected by optical sensors. As seen in figure 1, SAR imagery clearly highlights water features that optical sensors struggle to pick up. SAR is an all-sky sensor, meaning that it operates regardless of light conditions. Its wavelength range is also large enough that it penetrates cloud cover. This combination of traits helps provide continuous spatial coverage in geographic areas that might otherwise be occluded to optical satellite sensors due to cloud cover [15], or polar regions that lack sunlight for half of a year.

SAR is predicated by passive microwave sensing, which monitors similar microwave frequencies in order to pierce cloud cover but does not emit a signal of its own in order to do so. As a result, passive microwave sensing offers much

lower resolution compared to SAR. Sensors such as AMSR [113], AMSR-2 [1], SMAP [38], and GPM [88] all passively monitor microwave signals emitted from the Earth. By comparison, SAR actively beams energy down to Earth's surface and records the response, which allows for multiple polarizations at transmission and reception. Polarization describes the orientation of the plane that the electromagnetic wave oscillates on. The shorthand for polarization is the orientation of the emission, which is either vertical (V) or horizontal (H), followed by the orientation of the reception, which will also be either vertical or horizontal. Each polarization results in the waves scattering differently upon reflection, enabling certain polarizations to be particularly effective at picking up certain types of surface features. For example, the VV polarization is good at picking up rough surface scattering, typically caused by roughened water or vertical surfaces. HV or VH polarizations are good at picking up volume scattering, where the signal bounces around a number of times in a given volume before being broadcast back out to space. This is typically caused by forest canopies and vegetation. We see in figure 1a and figure 1b that the VH polarization provides more fine-grained details in a variety of forested areas than the VV polarization, where those areas are whited out. HH polarization is good at picking up horizontal surfaces, such as smooth ice or calm water.

Compared to optical imagery, SAR captures distinct and complementary information, despite it also being stored as a raster (gridded) data type. The different frequencies of SAR, the different polarizations, and the volume scattering aspect make it stand apart from optical. For instance, surface reflectance of sea ice will appear as a bright surface in optical imagery, regardless of its age (which is a proxy for its thickness and the level of hazard it poses to marine navigation). However, as sea ice ages (from thinner first-year ice to thicker multi-year ice), its salinity changes. Because of SAR's volume scattering (caused by salt content and air bubbles in ice), the appearance of thick ice changes in SAR imagery compared to younger, thinner ice [95]. This is the primary reason sea ice analysts rely on SAR imagery in making sea ice charts and use optical only as a secondary reference. As we demonstrate later in this manuscript, this complementary aspect of SAR imagery (despite it being stored as an image) motivates incorporating this multi-sensor information into RS foundation models.

3.3 Non-Image Data

Due to the ubiquity of the raster image format in remotely sensed data, current RS foundation models tend to be focused on using images to train, but a variety of other modalities do exist. Text, geographic location, and digital elevation maps (DEM) are all among potential additional modalities available in remote sensing at scale. It is conceivable that derivative information products such as population movement trajectories, social media data, and vector maps may be incorporated in enhancing foundation models. Any dataset with sufficient spatial coverage that contains geographic coordinates and a timestamp can feasibly be compared with corresponding satellite imagery. Such comparisons would further improve a model's ability to interpret how satellite imagery pertains to ground level information. This spatiotemporal relationship results in a broad swathe of different modalities available for RS models to leverage. With an eye on these additional potential modalities, the rest of this manuscript focuses on the present and immediate future of foundation models in remote sensing.

4 Foundation Models Originating in Computer Vision

This section presents a broad overview of the techniques used by current foundation models in CV, many of which serve as the bedrock for RS foundation models today [80].

4.1 Negative Sampling Models

One successful approach to SSL in CV is contrastive learning via negative sampling [23]. Contrastive learning augments one image in two different ways, then a model is trained to recognize whether two images are augmentations of each other, i.e., are a positive pair. Any images that are not augmentations of one another are defined as negative pairs. For every batch, an image will have only one positive pair, and $n-1$ negative pairs, where n is the batch size. This approach can be thought of as a classification task where the model trains on classifying two augmentations as either a positive or negative pair. Within a given batch of samples, normalized-temperature cross entropy loss (InfoNCE Loss) [23] pulls together embeddings from the same original image and pushes apart embeddings that came from different images. This results in an encoder that learns sophisticated embeddings of images without the need for supervised learning. The encoder then can be ported to other downstream tasks, while reducing the need for labeled samples.

SimCLR [23] achieved great success with this approach. SimCLR trained on ImageNet ILSVRC-2012 [104] and introduced a non-linear projection head to improve the embedding quality of the layer before it. They also discovered that augmentations like color jitter and random cropping were particularly effective in forcing the model to learn embeddings that represented the data as a whole. Training without augmentations resulted in a model that learned dominant features, such as color distribution, and were able to trivialize the SSL task. Momentum Contrast (MoCo) [50] also utilizes contrastive learning, but maintains a dynamic memory bank or queue of negative samples, and updates it using a momentum encoder. This approach allows MoCo to effectively utilize smaller batch sizes than SimCLR, reducing memory requirements. Contrastive Language Image Pre-training (CLIP) [98] is a contrastive learning framework that utilizes image captions as a way to supervise learning image representations. CLIP trains two encoders, one for the text modality and one for the image modality. Given the multi-modal nature of this approach, contrastive learning to bring positive pairs together results in an alignment of the two modalities in the same embedding space. All of these models introduce concepts that have been leveraged by recent foundation models within the RS domain [124].

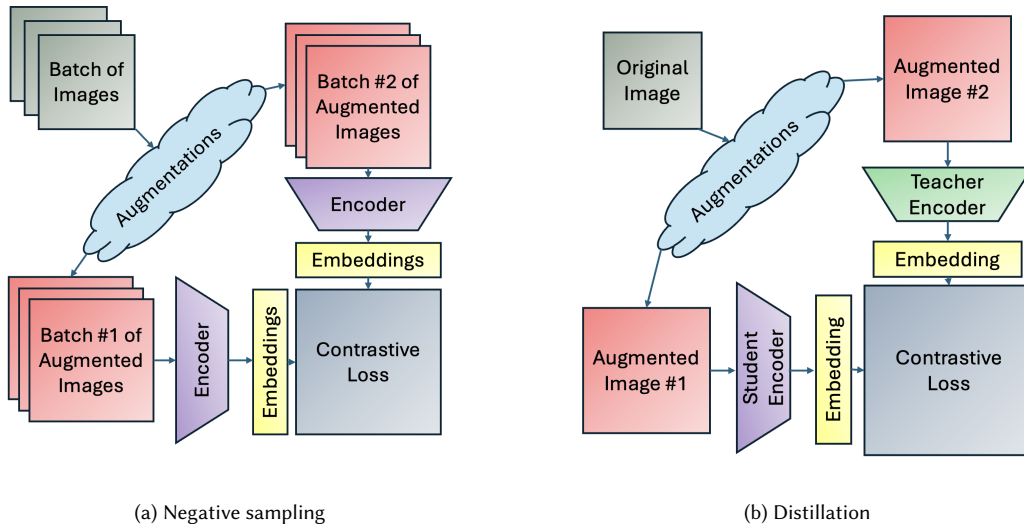


Fig. 2. CV foundation model architectures that leverage contrastive learning.

4.2 Distillation Frameworks

While contrastive learning via negative sampling achieves SOTA performance in CV, it generally requires large batch sizes. The number of negative pairs increases exponentially with relation to the batch size, and negative pairs are a key component of InfoNCE loss. This need for a large batch size results in significant hardware requirements, which is an obstacle to research for many teams. Distillation networks such as Bootstrap Your Own Latent (BYOL) [46] and Self-Distillation with No Labels (DINO) [18] were developed in part to address those hardware constraints.

Distillation simply refers to the concept of one model being trained on the outputs of another model [94]. Distillation is not strictly an SSL method, as some research focuses on using distillation to 'compress' knowledge from a large pre-trained model into a smaller model [129]. Distillation leverages two encoders, dubbed the "teacher" and the "student". When trying to 'compress' logic, the teacher is some pre-trained model, but in the context of SSL, both student and teacher encoders are learning, albeit not at the same rate or with the same method, depending on the specific set up. Both are fed in augmented versions of an image to output embeddings. Then, contrastive loss is performed between the teacher and student embeddings and back propagated through the student network. The teacher network typically learns via the weighted average update system that was introduced in MoCo [50]. Distillation models such as Joint-Embeddings Predictive Architecture (JEPAs) [4] build on this framework by introducing a decoder after the student to predict the embeddings from the teacher. This approach leverages reconstruction loss in the latent space, but more distillation SSL approaches rely on contrasting embeddings from the student and teacher encoders [27, 46, 62, 93].

The distillation methodology reduces the reliance on large batch sizes and extensive memory, making it more resource-friendly. It also outperforms comparable negative sampling models with fewer parameters [46]. However, there is possibility of embedding collapse, as both the teacher and student networks learn based on the same loss [24]. Embedding collapse describes a condition where a model generates embeddings that span a low-dimension subspace of the latent space, sometimes becoming so extreme as to only span a single point; this represents a significant loss of ability to capture information in embeddings [64]. Frameworks introduce asymmetry through weighted average loss for the teacher [50] or an additional decoder for the student [46]. This asymmetry between student and teacher is designed to prevent embedding collapse, but this phenomena is still an active area of research [59].

4.3 Redundancy Reduction

Like the two contrastive approaches discussed above, redundancy reduction creates augmented views of an image and passes those views through an encoder to generate two embeddings, which it then attempts to align. But instead of simply aligning embeddings within the latent space, redundancy reduction generates an empirical cross correlation matrix between the two embeddings. The matrix is $N \times N$, where N is the number of dimensions in the latent space, and each value ranges from -1 (perfect anti-correlation) to 1 (perfect correlation). Redundancy reduction loss is designed to make the resulting cross correlation matrix resemble the identity matrix.

Redundancy reduction approaches can differ in exactly how that loss is calculated. Barlow Twins [136] utilizes two terms: an invariance term and a redundancy reduction term. The invariance term forces the diagonal of the matrix to values of 1, while the redundancy reduction term forces the non-diagonal elements of the matrix to values of 0. This shares similar goals to InfoNCE loss, where the invariance term draws embeddings closer together (like positive pairs), and the redundancy reduction term forces embeddings further apart (like negative pairs). However, InfoNCE loss does this across a batch of embeddings, whereas Barlow Twins' loss does so within a given embedding. VICReg [10], builds on Barlow Twins' intuition and includes three terms: a variance term to prevent collapse, an invariance

term based on mean squared error between paired embeddings, and a covariance term to reduce redundancy among feature dimensions.

Redundancy reduction approaches, like distillation SSL, do not require as large of a batch size compared to negative sampling in order to learn effectively [10]. Barlow Twins also demonstrated an intriguing ability to more effectively leverage very-high-dimension embeddings: performance increased linearly with regard to the number of dimensions in the latent space. This trend was observed up to a latent dimensionality of 16K. [136].

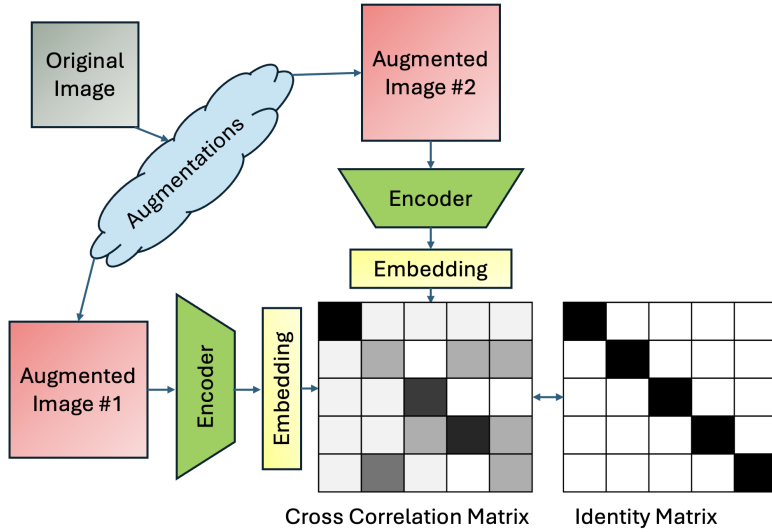


Fig. 3. An illustration of a CV foundation model that relies on redundancy reduction.

4.4 Masked Image Modeling

Masked Image Modeling (MIM) refers to self-supervised frameworks that reconstructs masked portions of an input image. MIM is inspired by the Masked Language Modeling (MLM) paradigm introduced in BERT [36]. It is worth noting that this is different from autoregressive models such as GPT [99], which learn to predict the next token in sequence rather than reconstruct masked inputs.

MIM generally entails the following steps:

- (1) Parts of a sample are masked.
- (2) The masked sample is run through an encoder to generate embeddings.
- (3) A decoder is asked to reconstruct the original sample from those embeddings.

Within MIM, several approaches have emerged beyond the widely used Masked Autoencoder (MAE) framework [49], including BEiT [9] (which predicts discrete visual tokens from a pre-trained tokenizer), SimMIM [131] (which reconstructs raw pixels of masked patches directly), and iBOT [140] (which predicts masked patch embeddings through self-distillation). These differ primarily in their masking strategies, prediction targets, and encoder-decoder configurations. While the CV literature now spans this diversity of masked modeling techniques, MAE tends to be a

popular option. Research in remote sensing has so far focused mainly on MAE-style methods due to their scalability and efficiency on large unlabeled satellite datasets [49], while incorporating ideas from other approaches to enhance representation learning. As such, we will tend to put central focus on MAE within the context of this paper.

MAE masks roughly 75% of the data to prevent trivial reconstruction from patch context [49]. The generative nature of the task means that the batch size can be relatively small, making it resource-friendly. MIM approaches with established frameworks, such as Convolutional Neural Networks (CNNs) or Recursive Neural Networks (RNNs), replace a patch with a mask token, then feed in the whole image, including masked patches, into a network. But in MAE, the usage of ViTs allows for training pipelines to only feed encoders unmasked patches. Positional embeddings, in addition to patch embeddings, allows the ViT to avoid processing masked tokens. This shrinks the size of the necessary input layers and dramatically speeds up training time [49]. Similarly, utilization of a lightweight decoder also forces the encoder to learn more accurate representations while speeding up runtime [49]. These optimizations mean that the MAE approach scales remarkably well, resulting in models that can contain billions of parameters [35]. Current CV research has identified a gap in the number of parameters between SOTA NLP and CV models. There are plans to improve the parameter count in CV foundation models even further [35].

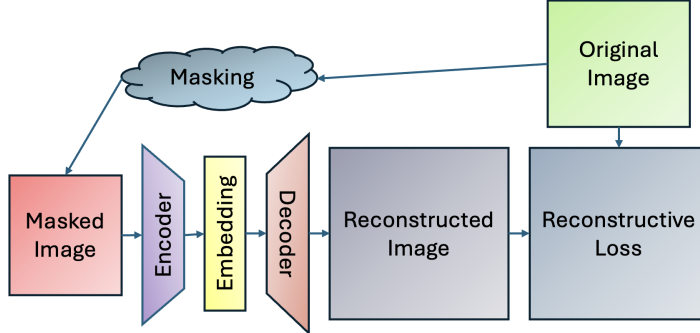


Fig. 4. CV foundation model framework for masked image modeling

5 Negative Sampling Models in Remote Sensing

While the underlying principles of negative sampling generally remain the same from CV to RS, RS images often share temporal or geospatial qualities. [59]. For example, Sentinel-1 and Sentinel-2 satellites can have images taken of the same location during the same day. These shared spatiotemporal attributes enables two potential advantages for RS foundation models:

- (1) Models can leverage imagery that comes from different RS sensors or different temporal acquisitions as naturally occurring augmentations.
- (2) It reduces the time required to do hyper-parameter tuning for augmentations.

The latter often adds significant overhead to training contrastive learning approaches [60].

5.1 Temporal Pairing

Pre-trained on RGB bands from Sentinel-2, Seasonal Contrast (SeCo) [84] borrows heavily from SimCLR’s general framework and outperforms CV models such as MoCo on downstream land cover classification tasks. This indicates that there is implicit benefit in creating foundation models for the remote sensing domain as opposed to borrowing models directly from the CV field. Instead of only using hand-crafted image augmentations outlined in SimCLR [23], such as color jitter or gaussian blur, SeCo treats images of the same location at different points in time as natural augmentations of one another. However, SeCo does not simply rely on these natural augmentations. It also utilizes random cropping, random flipping, and color jitter to prevent the model from learning trivial representations of the data. The resulting model is essentially season- or time-agnostic, meaning it provides a general representation of data regardless of acquisition-time-of-year. This is helpful in seasonally invariant tasks, such as identifying land cover. However, it may not fit scenarios where retaining seasonal differences in embeddings for downstream tasks is essential, such as projecting forest fire recovery in an area.

SeCo’s approach of contrastive learning between spatially aligned, temporally different RS image pairs has also been explored in Geographically Aware Self Supervised Learning (GASSL) [6]. However, GASSL trains on the Functional Map of the World (FMoW) [29] dataset, which contains multispectral imagery from the DigitalGlobe constellation [2], and does not utilize any additional artificial augmentations. In addition to the contrastive task, GASSL also leverages the metadata available in RS imagery for a SSL task. This approach clusters together images by location and then predicts the latitude and longitude present in the metadata. The combination of this task coupled with contrastive learning across geographically aligned images results in a framework that attempts to explicitly learn time-agnostic representations of a given place. As with SeCo, the authors note that this approach learns temporally invariant features, and may struggle with tasks such as change detection [6]. Unlike the approaches below, latitude and longitude are not pre-processed in any way or treated as an additional modality.

5.2 Geolocation Pairing

Explicitly utilizing spatial data such as latitude and longitude provides value, but purely introducing them as features can result in models that perform poorly when asked to generalize to locations not within their training data [67]. Therefore, a new generation of models dubbed “location encoders” have emerged. Once trained, a location encoder can take in latitude and longitude and return an embedding of that location which quantifies and summarizes ground conditions present there. Several models in this generation of location encoders rely on the CLIP framework [98] and treat ‘location’ as one modality, with a location-specific encoder to use in contrastive learning. This location encoder, in turn, learns the information extracted from the other mode, often an image obtained at that location.

GeoCLIP [20] uses images taken at ground level from Flickr for one modality and spatial encodings for the other modality. GeoCLIP then uses CLIP’s contrastive learning objective to learn effective representations of each modality. GeoCLIP uses Random Fourier Features (RFF), which have been shown to be highly effective in memorization and image reconstruction [114], in order to store features learned from images into the location encoder. These Random Fourier Features allow GeoCLIP to learn high quality spatial encodings that capture information from the ground level photos.

Contrastive Spatial Pretraining (CSP) [83] also performs contrastive learning between ground level imagery and locations, but it explores a variety of techniques for generating positive and negative pairs that are explicitly tailored to

spatially distributed data. In addition to CLIP’s standard in-batch negative sampling, CSP utilizes random negative location sampling, in which negative pairs for an image are generated by uniformly sampling locations at pre-training time. In this instance, the positive pair is still the corresponding location for the image. CSP also explores SimCSE-based sampling [44], in which two location encoders are initialized the same, but utilize different dropout masks. In this case, the same location is fed through each location encoder, and embeddings that point to the same initial location are considered positive pairs. All other combinations are considered to be negative pairs. Each sampling approach forms a component of CSP’s contrastive loss function, resulting in a framework that learns nuanced representations of each modality. CSP trains on ground-level imagery from the iNaturalist dataset [120].

SatCLIP [67] also follows the CLIP approach while utilizing spatial encodings as one of its modalities and optical imagery captured from Sentinel-2 as the other. SatCLIP takes in all Sentinel-2 bands and does not limit itself purely to RGB data. SatCLIP does not utilize Random Fourier Features for the spatial encodings, and instead uses a SirenNet [107] that relies on spherical harmonics [105] to learn effective spatial encodings.

Geo-Aligned Implicit Representations (GAIR) [76] takes this a step further by utilizing location as a way to align multispectral satellite images from Sentinel-2 and ground-level RGB images from the Global Streetscapes dataset [55]. Ground-level imagery can provide a highly informative mode to train satellite imagery against. However, a single satellite image’s scope is so large that hundreds or thousands of ground-level images can correspond to a single satellite image. In order to address this issue from a contrastive learning standpoint, GAIR learns Implicit Neural Representations (INR) [134] of a Sentinel-2 image. INR learns a continuous function for spatial coordinates to corresponding signals. These INR encodings of Sentinel-2 imagery are then contrasted against location encodings and ground level vision encodings. GAIR uses RFF [114] for location encodings and a standard ViT for ground-level image encodings.

5.3 Multisensor Pairing

Multi-modal SimCLR [60] treats images of the same location from different sensors as naturally occurring augmentations. This approach has two encoders: one trained on RGB bands of Sentinel-2, and one trained on VV and VH polarizations of SAR images from Sentinel-1. As with SeCo, this approach does not rely entirely on natural augmentations. It adds random cropping, flipping, color jitter/drop, and gaussian blur, all augmentations that have proven useful in other remote sensing models [59]. Interestingly, fine-tuning Multi-modal SimCLR on downstream tasks with a dataset of only one modality, either Sentinel-1 or Sentinel-2, yields better results compared to other methods that train only on the one sensor [60]. This indicates that leveraging the additional modalities (i.e., sensors) present in remote sensing for SSL has the potential to result in better representations of a single modality in the modality-specific encoder.

5.4 Image-Text Pairing

CLIP’s original design used text and images as its two modalities, and RemoteCLIP [75] goes back to these roots. RemoteCLIP takes in text as its one modality, leaning on image captions to generate natural labels. Other models’ requirements for additional fine-tuning, as opposed to zero-shot utilization, motivates this model’s development. Including text as one of the modalities results in good zero-shot performance downstream [143]. This model treats RGB images taken from Sentinel-2, drones, and other aerial platforms as one modality. This variety in the sources for the image modality is designed to result in a more robust encoder that will be resolution agnostic. RemoteCLIP’s reported underperformance in zero-shot image classification tasks indicates that there is additional work to be done in that regard.

For the text modality, RemoteCLIP relies on image captions already present in the human-annotated satellite imagery datasets. Where no captions are paired with an image, a preprocessing stage generates appropriate text annotations. This preprocessing stage performs standard object detection on the image, then uses a script to programmatically generate a corresponding sentence. That sentence is then used as the positive text annotation. Generating captions via script will lack natural variance that is present in a typical corpus, and generating these captions via NLP processes such as ChatGPT will inherently introduce extrinsic noise and potential bias into the dataset. Nevertheless, RemoteCLIP outperforms SOTA models like CLIP and DINOv2 in zero-shot evaluation of object counting in the Remote-Count dataset [43], and few-shot classification of 12 RS benchmarks, including EuroSat [52], RSC11 [139], and RESISC45 [28]. This performance indicates that text as a modality has definite value in the remote sensing domain.

Given multi-modal foundation models' origins as VLMs, there are a variety of other RS foundation models that leverage text as a modality in order to enable few-shot learning capabilities. These models have been surveyed by [141].

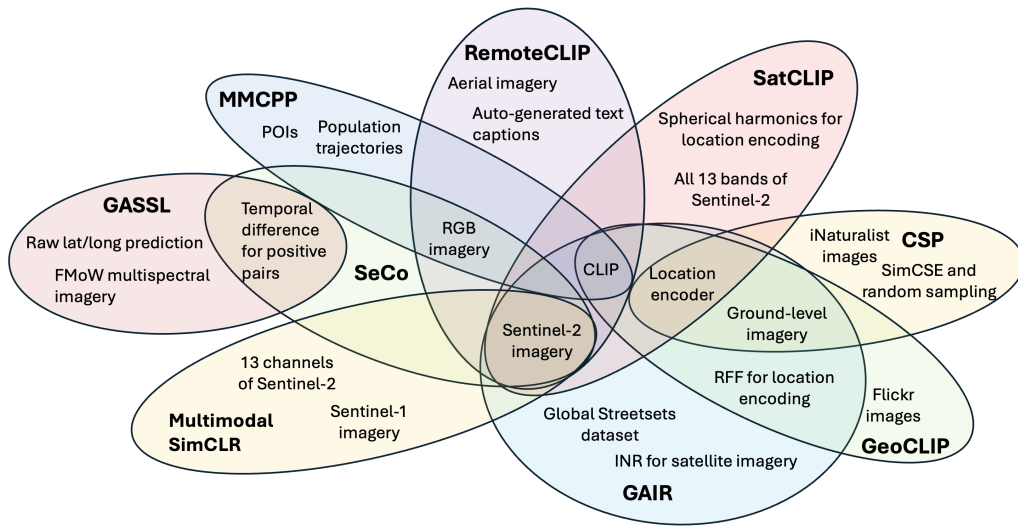


Fig. 5. An illustration of shared and unique concepts among RS foundation models which utilize contrastive learning with negative sampling for their SSL task.

6 Distillation Networks in Remote Sensing

Given the requirement for handling a sizable amount of remotely sensed data, efficiency-oriented SSL approaches like distillation have become popular for remote sensing foundation models.

6.1 Sensor-Agnostic Encoder

One successful example of a distillation network in the RS field is RS-BYOL [60], which borrows BYOL's framework and uses the multi-modal aspect for multi-sensor remote sensing data. Just as with negative sampling approaches in RS, different sensors' imaging of the same location are leveraged as natural augmentations of the same image. One modality is drawn from Sentinel-2 optical, whereas the other is drawn from Sentinel-1 SAR. Similarly, additional augmentations of random crops, rotations, color jitter, and grayscale are applied to prevent the model from learning

trivial representations of the data. RS-BYOL utilizes 10 bands of data in Sentinel-2 with 10-20 m resolution and the VV and VH polarizations of SAR present in Sentinel-1. RS-BOYL only trains a single encoder at a time and chooses 3 random bands of Sentinel-2 and 3 random polarizations from Sentinel-1 to make up the two image views. They perform distillation with view 1 passing through the student encoder and view 2 passing through the teacher encoder, then also perform distillation with the views passing through the opposite encoders. The resulting framework represents an early attempt to learn sensor-invariant features.

The model outperforms negative sampling approaches such as SeCo in linear probing when all bands are present from Sentinel-2, indicating that there is inherent value in incorporating multispectral bands from Sentinel-2 in addition to the RGB bands. However, SeCo outperforms RS-BYOL with linear probing when only the RGB bands are present, indicating that negative sampling approaches may still have a performance edge in remote sensing. The lighter resource requirements for distillation networks reflects a tradeoff between model performance and hardware requirements. RS-BYOL represents a somewhat straightforward adaptation of CV distillation SSL techniques in RS, but other approaches make more dramatic changes.

DINO-MM [125] is another RS foundation model leveraging distillation as its SSL objective, although this model is built off of DINO's [18] framework instead. DINO-MM trains on BigEarthNet-MM [111], a dataset containing roughly half a million pairs of Sentinel-2 and Sentinel-1 images at the same spatiotemporal scenes. DINO-MM represents one of the first RS foundation models to explore the use of ViTs [37] as a backbone. As such, its student and teacher encoders can handle flexible input shapes. DINO-MM takes full advantage of this, stacking SAR and MS channels on top of one another to create the 'original image'. DINO-MM applies the standard augmentations present in DINO, but also introduces a RandomSensorDrop augmentation that results in one of three outcomes:

- (1) All SAR channels are dropped
- (2) All MS channels are dropped
- (3) No channels are dropped

This results in an encoder that is capable of leveraging whatever satellite imagery is available when creating embeddings. In theory, it also means that this model learns intra- and inter-modal representations of the data. However, this framework's flexibility does not necessarily guarantee performance when all modes of data are present. Reported ablation studies show that downstream assessment on BigEarthNet's classification task perform well with Sentinel-2 data, but do not actually improve when given additional Sentinel-1 information. In the case of top-1 benchmarking, the model's performance actually decreased slightly while fine-tuning on Sentinel-1 and Sentinel-2 imagery (when compared to purely Sentinel-2 fine-tuning). It is possible that benchmarking on tasks where SAR data is more relevant, such as Sen1Floods11 [12], might yield more favorable results with multiple modes of data present.

6.2 Multiple Contrastive Tasks

SkySense [47] represents a significant step in RS foundation model size, with 2.09 billion trainable parameters. Aside from model size, SkySense performs distillation SSL at multiple stages of its training pipeline, resulting in a model capable of learning effective high level and low level features. SkySense trains on three modalities: time series of Sentinel-1, time series of Sentinel-2, and high resolution RGB imagery from Worldview 3 and 4. For each mode, there is a teacher and student encoder. SkySense performs two sets of random augmentations per image, then sends the different views to the student and teacher. It performs multi-modal contrastive loss between the embeddings from the

student encoders and then performs a number of contrastive learning tasks between student and teacher embeddings, namely:

- pixel-level contrastive loss
- image-level contrastive loss via average pooling of pixels
- object-level contrastive loss by using the Sinkhorn-Knopp algorithm [68] to perform unsupervised clustering on pixel-level features

After these contrastive tasks, the embeddings go through a multi-modal temporal fusion encoder at both the student and teacher level. This results in a fused embedding. Sinkhorn-Knopp is applied again, but this time, the resulting clusters are compared to geographic regions in order to learn geo-context. Then the fused embeddings go through the same contrastive learning tasks described in the paragraph above. The resulting model was reported to achieve SOTA performance on downstream tasks.

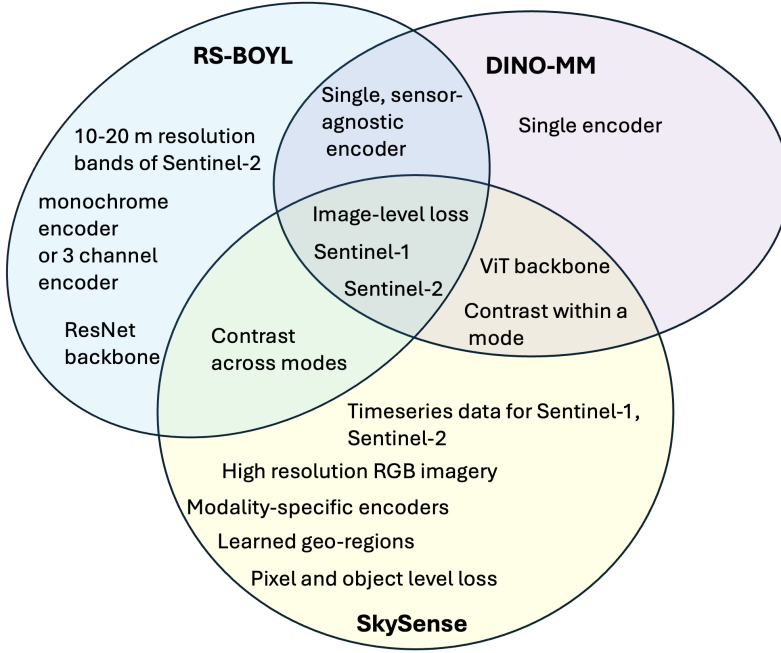


Fig. 6. An illustration of shared and unique concepts among RS foundation models which utilize knowledge distillation for their SSL task.

7 Redundancy Reduction in Remote Sensing

Decoupling Common and Unique Representations (DeCUR) for Multimodal SSL [123] builds on the Barlow Twins redundancy reduction approach, but modifies it to handle multiple modes of data. DeCUR explores several multi-modal training datasets. In order to explore the efficacy of their multi-modal training approach, DeCUR trains one model per each of the following datasets:

- SAR/optical imagery from SSL4EO [126]

- RGB imagery/DEM data from GeoNRW [7]
- RGB imagery/depth data from SUN-GRBD [109]

DeCUR’s key distinction from other multi-modal approaches we have discussed lies in its desire to learn inter-modal representations, but preserve data unique to a given modality. It does so by setting aside a percentage of the latent space for shared representations and leaving the other percentage of the latent space for modality specific information. When the Barlow Twin’s redundancy reduction loss is applied from one mode to another, DeCUR only calculates this loss for shared dimensions of the latent space. DeCUR also calculates redundancy reduction loss within a given mode itself, and does so for all of the dimensions within the latent space. This strategy enables DeCUR to align modalities without losing modality-specific information and results in SOTA performance on downstream tasks.

One potential downside of this approach is the calculation of the shared latent space dimensions. The authors use a light grid search in each dataset to determine how much of the latent space should be used for learning shared representations. This percentage tends to hover around 75-80% in the datasets above, but calculating it becomes costly with larger datasets. The authors also found no significant drop in performance when they dropped the shared dimensions to as low as 50%. This suggests a degree of sparsity in the shared latent space and an opportunity to refine how the shared dimension percentage is calculated, or ways to even better leverage all dimensions.

8 Masked Image Modeling in Remote Sensing

While MIM is a powerful approach in CV, there is significant room to optimize performance for remotely sensed imagery. Below are some of the adjustments that have been made to MIM in order to leverage it more effectively in the remote sensing domain. Most models discussed follow the MAE masking and decoder paradigm, with a few noted exceptions.

8.1 Masking Approach

The simple CV approach of masking individual patches of an image can work with RS imagery, but there is room for improvement [112]. Compared to natural images in CV, satellite and aerial images in RS often capture small surface features, dense objects, complex backgrounds, and a range of possible object orientations. Similarly, natural images tend to follow expected proportions with well-defined distributions, whereas the same cannot be said for RS images [101]. Sun’s Remote Sensing Foundation Model (RingMo) introduces PIMask [112] to account for these inherent differences, as masking an entire patch of a RS image might lose information that is unique to that given patch. Therefore, some pixels in each masked patch are randomly preserved, and multilayer convolution is applied to each patch. Compared to traditional CV methods, where masking 50% of an image would completely mask 50% of the patches, masking 50% of an image with PIMask would partially mask a higher percentage of patches. The overall number of pixels masked in the image would still be 50%, but the spatial distribution is different. RingMo is officially classified as a MIM approach, as the masking strategy does not allow for the encoder to only be fed unmasked patches.

MAE in CV finds that masking high percentages of the image (roughly 75%) results in more accurate representations being learned [49], and that carries over to the current implementations of MAE in remote sensing as well [112]. This parallels with the findings from negative sampling approaches that making the pretext task with contrastive objective more difficult via multiple augmentations results in the model learning better embeddings. RingMo’s embeddings outperform embeddings generated with comparable MIM frameworks and standard CV patch masking, underscoring the importance of improving the masking procedure for satellite imagery.

Spatial-Spectral MAE (S2MAE) [73] takes this a step further, as they find that masking 90% of satellite imagery yields the best results in their novel framework. S2MAE trains on multispectral imagery from FMoW [29] and BigEarthNet [111] datasets. Unlike RingMo and other image RGB masking strategies which mask out the same pixel across all channels, S2MAE employs independent 3D masking, which masks out different pixels in each channel. 3D masking was introduced for videos and appears to learn environmental details well, but struggles to track movement from frame to frame [40]. While this is poorly suited for video analysis, it is ideal for RS applications, as seen in S2MAE's SOTA performance on the Onera Satellite Change Detection (OSCD) [34] and EuroSat [52] benchmarks. S2MAE also finds that shallow decoders are poorly suited for MAE with multispectral imagery, a notable departure from established CV practices [49].

SatMAE [32] also experiments with different masking approaches. It utilizes consistent masking, where the masked regions are spatially-consistent across all images of a given location, and independent masking, where the location of the patches can change from image to image of a given location. Results indicate that independent masking can trivialize the task by leveraging spectral redundancy. In other words, the model might be able to reconstruct a given masked patch by referring to an unobstructed view of that patch at a given time. A random cropping augmentation is applied to address this and ensure the model learns robust embeddings.

SpectralGPT [54] experiments with a unique 3D-cube masking strategy. Training on 12 bands of Sentinel-2 data from FMoW [29] and BigEarthNet [111], SpectralGPT's approach cannot be described as either independent or consistent masking. Instead of tokenizing channel by channel, SpectralGPT creates non-overlapping tokens which span 3 channels. Independent masking is then applied to each layer of tokens. This results in a blend of consistent and independent masking that is informed by spectral resolution. SpectralGPT also uses multiple loss terms in their approach, generating loss based on token-to-token reconstruction, but also spectral signature-to-spectral signature reconstruction. Similar to S2MAE [73], SpectralGPT finds that it performs best with a masking rate of 90% and a deeper decoder.

8.2 Temporal Encodings

SatMAE [32] leans on MAE's utilization of a ViT as the backbone, but encodes the hour, month, and year as temporal encodings. SatMAE then concatenates these temporal encodings to the standard positional encodings that are innate to the functioning of a ViT. As with SeCo, the inclusion of temporal information in self-supervised learning for RS foundation models can have substantial performance improvements, but it also means that the embeddings learned are agnostic to temporal variability. Thus, the embeddings' applicability to temporally sensitive downstream tasks is limited. Still, this ability to encapsulate temporal data highlights the flexibility of the MAE approach in remote sensing.

Prithvi [61] trains on the Harmonized Landsat Sentinel-2 (HLS) [31] dataset, which contains multispectral images captured by Landsat 8/9 and Sentinel-2. Given the differing revisit times of the two satellites, HLS is a satellite imagery dataset with a high temporal resolution. Prithvi leverages this higher temporal resolution to arrange these 2D images in a time series and updates the traditional MAE positional and patch embeddings to be 3-dimensional, where the third dimension pertains to time. When masking patches, they specifically apply 3D convolutions to avoid losing information specific to any one given patch, similar to RingMo's [112] approach. Unlike RingMo, Prithvi fully masks patches. Prithvi also utilizes a landscape stratified sampling strategy to avoid bias towards more common ecosystems or landscapes.

Presto [118] takes this approach even further, constructing a pixel-timeseries training dataset that consists of input from multiple types of data, including Sentinel-2 RGB, Sentinel-1 SAR, DEM, and the Dynamic World [14] dataset. Dynamic World contains land cover labels for 10m resolution Sentinel-2 imagery. The framework then employs a variety of different strategies for training. It masks channels, blocks of timesteps, single timesteps, and/or random pixels

for reconstruction by a downstream encoder. The resulting encoder performs well on feature extraction, fine-tuning, and time series forecasting. The variety of masking strategies ensures that Presto can successfully process time series datasets with missing channels, a variety of temporal resolutions, and only a small subset of timesteps. However, performance on tasks that are temporally agnostic and rely on a single image lags behind SOTA models. The authors note that this is possibly due to the model’s inability to process images with a spatial resolution higher than 10m.

8.3 Spatial Resolution

Foundation models in CV, and most foundation models in RS by extension, process images in local image coordinates. This means that the learned representations are dependent on the spatial resolution of the satellite sensor. ScaleMAE [100] is designed to address this issue by scaling the image coordinate system such that it matches the actual spatial scale of objects, ensuring that patch size, as measured in geospatial units, is the same across various images. This is done via introducing a Ground Sample Distance (GSD) positional encoding, which then informs the ViT of both the geospatial scale and image position of the patch. Put differently, ScaleMAE addresses relative spatial resolution, but does not incorporate absolute geolocation in its training. As with SatMAE, ViT’s framework lends itself well to introducing the concept of spatial resolution to the model. Dovetailing with the incorporation of spatial resolution, ScaleMAE’s decoder produces both high and low resolution images in order to capture both low-frequency features, such as mountains and rivers, and more fine-grained high-frequency features, such as vegetation. It does so by utilizing a Laplacian-pyramid decoder [16] instead of the standard transformer decoder.

Where ScaleMAE focuses on understanding spatial resolution of the overall image, USat [58] chooses to focus on spatial resolution across image channels. Different bands of the same sensor can have dramatically different spatial resolutions. For instance, in the case of Sentinel-2, bands (i.e., input channels) range from 10m resolution to 60m resolution. Many approaches up- or down-sample channels to yield a consistent spatial resolution, and some simply drop low resolution channels altogether [59]. This ensures that patch sizes remain consistent, but may lose resolution specific information. USat trains on Sentinel-2 and NAIP, and adjusts the number of patches per channel depending on the spatial resolution. High resolution channels have more patches to capture specific high resolution information. Lower resolution channels have fewer patches, but the total number of patches must be evenly divisible by the number of high resolution patches. This enables channels with different resolutions to cleanly map to one another. Each channel will be masked by the same percentage. More patches are masked in high resolution channels to preserve the percentage of the image being masked. Then, patches are aggregated via spectral pooling, and a standard decoder is used to reconstruct the original image. This approach effectively extracts high-level and low-level features from differing resolutions, but does have some drawbacks. Namely, the assumption that different sensors will have a resolution that is cleanly divisible will not always be true. The authors also note that the approach becomes costly to train with multiple different sensors.

SatMAE++ [91] takes inspiration from ScaleMAE’s approach and seeks to introduce spatial resolution awareness to models that train on non-RGB modalities, training on Sentinel-2 imagery in FMoW [29]. They go about doing so with a more straightforward approach than ScaleMAE, doing away with GSD encodings and Laplacian Pyramid decoders. Instead, SatMAE++ has a multi-resolution reconstruction objective. An image is upsampled 2x and 4x, masking occurs, and then the same decoder is responsible for reconstructing different resolution images based on the corresponding masked input. For the original image, standard mean squared error is applied. For the upsampled blocks, L1 loss is used.

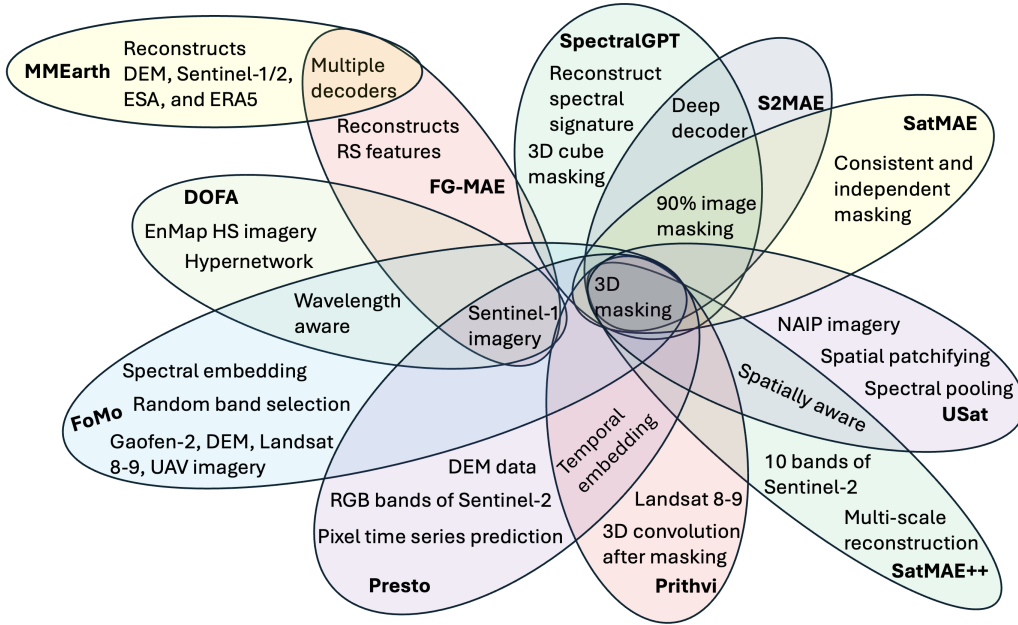


Fig. 7. An illustration of shared and unique concepts among RS foundation models which utilize masked auto-encoding for their SSL task and train on multispectral imagery from Sentinel-2 and potentially some other multi-sensor data.

8.4 Multiple Decoders

MAE is originally designed to take in a single modality, which can make it challenging to utilize the different sensors that are available in remote sensing. By comparison, contrastive learning models elegantly use different modes of data available by creating an encoder per modality. MMEarth [89] explores a potential multi-modal MAE approach by pairing an encoder for one modality with many modality or task-specific decoders. MMEarth takes in multispectral data from Sentinel-2 that contains all 13 bands, masks that data, then utilizes an encoder to generate embeddings. Typical MAE would pair this with a single decoder designed to reconstruct the original optical image. Instead, MMEarth pairs the optical encoder with 12 separate decoders. Six of these decoders are focused on pixel level tasks, such as reconstructing a corresponding optical image, a corresponding SAR image, or a corresponding Dynamic Earth image. The other six decoders are focused on image level tasks, such as classifying the corresponding biome or month.

The loss for all of these decoders is back propagated into the encoder, resulting in representations of optical imagery that capture data from other modes. While this approach learns refined optical representations, contrastive learning approaches of a similar manner would also learn representations for the other modes of data. Depending on the downstream modalities available, this may be a significant limitation for MMEarth's effectiveness.

Feature Guided MAE (FG-MAE) [127] also explores the utilization of multiple decoders for MAE, but does so by tasking the model to reconstruct specific features of interest in the remote sensing world. MAE's focus on pixel-level details can limit the model's capability in understanding satellite imagery. FG-MAE explores a variety of reconstruction objectives, including Histograms of Oriented Gradients (HOG) [33], Normalized Difference Indices (NDI) such as Normalized Difference Vegetation Index (NDVI) [56], CannyEdge [17], and Scale-Invariant Feature Transform (SIFT) [78]. FG-MAE maintains two separate models: one for optical imagery and one for SAR imagery. In EuroSat [52] and

BigEarthNet [111] classification tasks, FG-MAE’s optical model demonstrates comparable or better results to standard MAE when only reconstructing a single one of these RS features. However, performing reconstruction on both HOG and NDI results in a substantial performance boost compared to standard MAE. FG-MAE’s SAR model finds that simply reconstructing HOG yields the best results, as it tends to work well with the noisier Sentinel-1 imagery.

8.5 Orientation Awareness

In natural imagery, the orientation of objects is of importance; if an object is upside-down, that is semantically different compared to the same object right side up. By comparison, the same object can appear in satellite imagery in a variety of different orientations, and those orientations have little to no semantic differences. Leveraging the standard MAE approach from CV treats these orientations differently, which is not desirable for remotely sensed images.

Masked Angle-Aware Auto-Encoding (M3AE) [74] emerges to address this particular problem. M3AE trains on the MillionAID dataset [77], an RGB dataset derived from Google Earth imagery. M3AE introduces a scaling, center crop augmentation to every image, resulting in an augmented image where an object in the center will be rotated into a different orientation from the original. This augmented image is masked then fed into an encoder-decoder framework where the decoder attempts to reconstruct the original image. In order to ensure that the model pays attention to the re-oriented object, the encoder is fed positional embeddings that include a third dimension to track the angle of a given patch. M3AE also introduces an optimal transport reconstruction loss to automatically assign similar image patches for each rotated crop patch. This ensures that the rotation is taken into effect from a loss standpoint.

Rotated Varied-Size Attention (RVSA) [121] also develops a novel approach to developing orientation-agnostic representations of RS imagery, but does so through ViT self-attention compared to image augmentation. Trained on the MillionAID dataset [77], RVSA shifts away from the standard multi-head self-attention (MHSA) present in traditional CV ViTs, as full attention scales quadratically to image size. Given the potential high-resolution nature of RS imagery, RVSA leverages a varied-size window-based MHSA (VSA). In VSA, images are partitioned into non-overlapping windows, then have MHSA applied [137]. In order to learn orientation, RVSA randomly rotates and re-sizes these windows before performing self-attention within a ViT. With these self-attention tweaks in effect, standard MAE is employed for reconstruction masked MillionAID images. The result is a framework capable of swiftly handling high resolution RS imagery that learns orientation-agnostic representations of RS imagery.

While orientation matters a great deal for object recognition in RS imagery, the M3AE authors notes that this applies predominantly to man-made objects [74]. These representations are likely better suited for urban or developed environments, and development of a training dataset specifically focusing on man-made objects would likely be useful for model fine-tuning.

8.6 Wavelength Awareness

The variety of different satellite sensors available means that even if two sensors monitor the same rough wavelengths, their spectral resolution or means of acquisition might be very different. For example, Landsat-7 and Sentinel-2 are both considered multispectral and monitor visible to SWIR wavelengths, but Landsat-7 splits that into 8 distinct bands, compared to Sentinel-2’s 13 bands. As a result, a foundation model trained on Sentinel-2 data would not be well-suited to work with Landsat-7 data out-of-the-box, and vice-versa.

Dynamic One-For-All (DOFA) [133] attempts to address this problem by creating a framework that can take in data from any number of different sensors. DOFA follows a hypernetwork approach [22], where a hypernetwork takes in the wavelength details of a given band and then generates weights that are used to initialize a neural network. Image Manuscript submitted to ACM

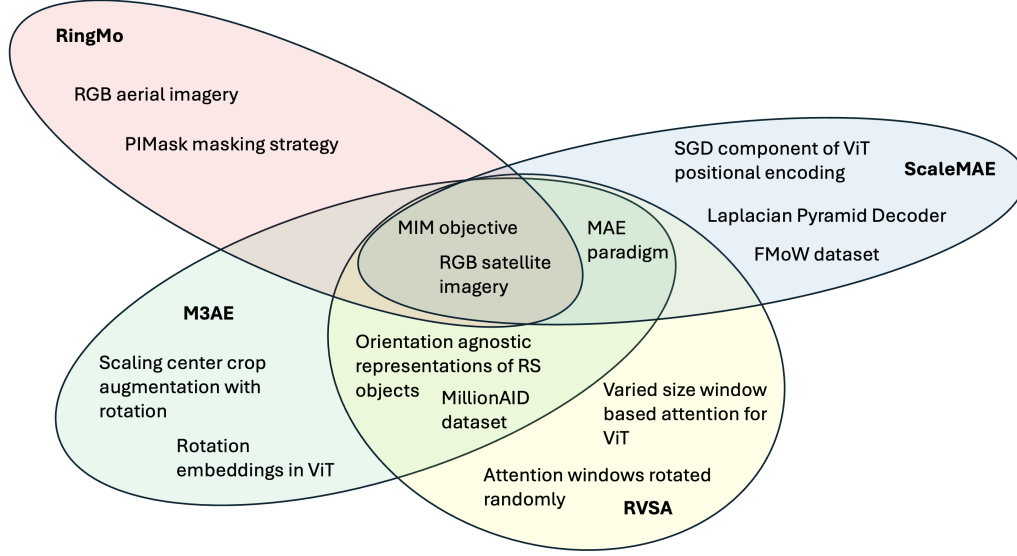


Fig. 8. An illustration of shared and unique concepts among RS foundation models which utilize masked image modeling for their SSL task and all train only on RGB images.

bands are masked, then fed into that neural network to generate encodings. The encodings are then fed through an encoder-decoder structure, with a mirrored hypernetwork at the end responsible for reconstructing the original image. This framework is designed to learn bandwidth specific features via the hypernetwork and shared features via the shared encoder-decoder. DOFA is trained on SAR imagery from Sentinel-1, multispectral imagery from Sentinel-2, hyperspectral imagery from enMAP, and high resolution RGB imagery from NAIP. The resulting framework achieves SOTA performance on downstream tasks such as BigEarthNet [111], So2Sat [142], and EuroSat [52].

While this framework is highly promising in its potential applications to downstream tasks on imagery acquired via a sensor not in the training set, this ability is unfortunately still largely theoretical, as it is not thoroughly explored in the published results [133].

Foundation Models for Forest Monitoring (FoMo) [13] also trains to be aware of spectral wavelength, but does so without the use of a hypernetwork. FoMo trains on four satellite-based datasets and four aerial-based dataset, with spatial resolutions ranging from less than 5cm to 60m. The datasets include MS imagery from Landsat 8-9, Sentinel-2, and Gaofen-2. They also include SAR imagery from Sentinel-1, DEM data, and both RGB and MS imagery from high-res UAV sensors. The resulting training dataset is rich in spatial and spectral diversity. FoMo's flexible training strategy groups together all of the images of the same spatiotemporal scene, then randomly selects bands to use in that particular sample. Each band is independently tokenized to avoid spatial resolution issues. FoMo then incorporates standard positional embeddings and introduces spectral embeddings to denote what band each channel belongs to. This setup allows for learned representations across bands and within bands. Tokens are masked, passed through a ViT encoder, and then go through a standard decoder for reconstruction. Due to the random band selection process for generating samples, batches can potentially be very different. Gradient accumulation across batches is used to 'smooth' the learning rate.

FoMo's architecture does not boast the ability to impute information for untrained on wavelengths the way DOFA might. However, the diversity of the training data and elegant approach yield a model that is effective at leveraging data from a wide swathe of sensors. The authors do note that independent channel tokenization can also lead to potential scalability issues. The amount of tokens per sample increases linearly with the number of spectral bands, resulting in the complexity of the self-attention mechanism increasing quadratically.

9 Combined Approaches

Several RS foundation models cannot in good conscience be described as falling into any of the above approaches. Instead, they leverage multiple objectives that span the approaches discussed above.

Contrastive Radar-Optical Masked Auto-encoders (CROMA) [41] is one such model. CROMA trains on Sentinel-1 and Sentinel-2 imagery and trains an encoder for each sensor. However, CROMA takes inspiration from the Fast Language Image-Pretraining (FLIP) framework [63], which independently masks each mode of data before feeding them into encoders and performing contrastive learning in the standard CLIP [98] setup. Masking images before encoding them results in a significantly less memory intensive process than encoding the raw image when vision transformers are used. Therefore, the FLIP framework enables contrastive training with a much larger batch size with the same or less memory footprint. This results in faster convergence. CROMA implements this approach with remotely sensed images, contrastively learning between masked Sentinel-1 and Sentinel-2 images. CROMA also introduces a third encoder that takes in concatenated Sentinel-1 and Sentinel-2 encodings to generate multi-sensor encodings. These fused encodings are fed into a multi-sensor decoder responsible for constructing the initial Sentinel-1 and Sentinel-2 images. In this manner, CROMA is able to introduce contrastive and reconstruction loss terms into their framework. This results in a model that effectively learns uni-sensor representations for Sentinel-1 and Sentinel-2 and multi-sensor representations of both Sentinel-1 and Sentinel-2. CROMA's framework is benchmarked against BigEarthNet [111] and FMoW [29] classification tasks, demonstrating SOTA performance with images from a single sensor and multi-sensed images. BigEarthNet contains roughly half a million Sentinel-2 images where each patch can have multiple land-cover classes. CROMA also utilizes modified Attention with Linear Biases (ALiBi) positional embeddings [97] for their ViT encoders. These embeddings provide an advantage over standard sinusoidal positional embeddings by biasing the embeddings based on Euclidean distance between key-query pairs, thus imbuing the embeddings with a degree of spatial awareness.

OmniSat [5] also leverages an encoder per modality, but does so for three separate modes of data:

- (1) timeseries of multispectral imagery
- (2) timeseries of SAR imagery
- (3) high resolution UAV imagery that features RGB bands, a NIR band, and DEM data

After patchifying and encoding the data through their respective encoders, OmniSat then performs contrastive loss between the patches of each modality, where each patch has $M-1$ positive pairs (M representing the number of modalities). However, OmniSat makes a key change to how it determines negative pairs, and denotes that any patches which neighbor the positive pair should not be considered as a negative pair. This may seem odd from the perspective of natural imagery, but within RS imagery, there tends to not be vastly different semantic information in neighboring patches. This follows Tobler's first law of geography: "Everything is related to everything else, but near things are more related than distant things" [86]. For the purposes of contrastive learning, it means that trying to use those neighboring patches as negative pairs will likely result in false negatives. This contrastive strategy addresses that false negative issue. OmniSat then performs independent masking, combines the latent representations into a multi-modal representation,

and then reconstructs the original image modes from the shared multi-modal representation. They choose MS timeseries reconstruction targets by considering the temporal attention maps. Lower self-attention scores indicate cloudy images, which make for poor reconstruction targets.

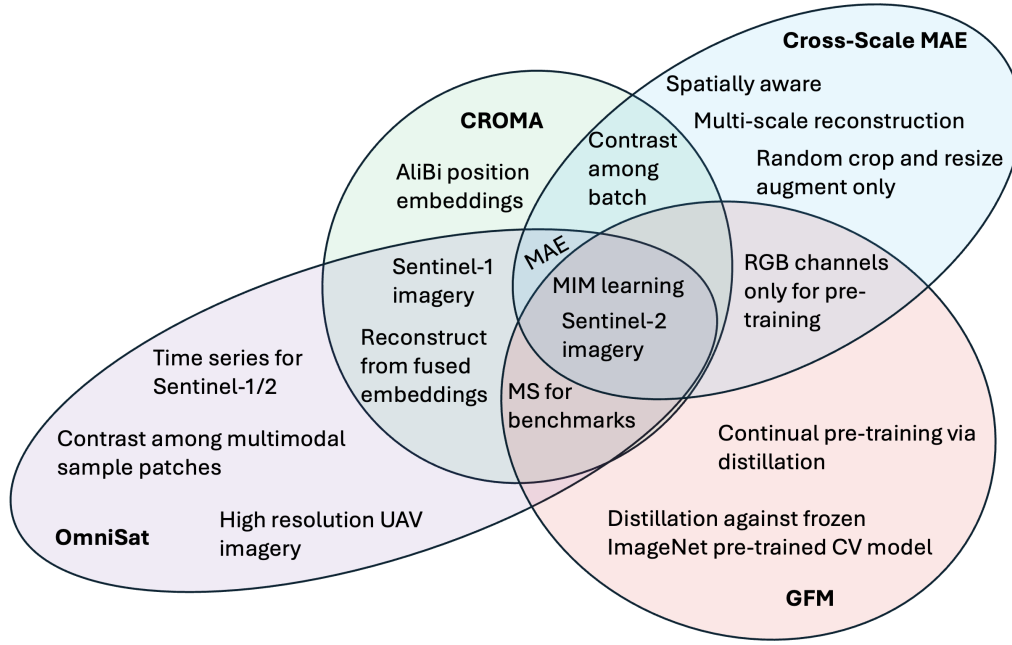


Fig. 9. An illustration of shared and unique concepts among RS foundation models which utilize hybrid learning strategies that combine contrastive, MIM, and distillation approaches.

Cross-Scale MAE [115] also leverages both contrastive and MAE approaches. Where OmniSat and CROMA use this combined approach to better train on multi-sensor data, Cross-Scale MAE does so in order to better understand spatial resolution. Trained on RGB data from the FMoW [29] dataset, Cross-Scale MAE performs a random crop and resize augmentation on a sample, then compares that to the original image. This comparison contains three components:

- (1) contrastive loss between embeddings of the original image and augmented image
- (2) mean squared error between the output of the attention block of the decoder for the original and augmented images
- (3) reconstruction loss of the original image (from a patchified version of the original) and augmented image (from a patchified version of the augmented image)

Contrastive loss between different spatial resolutions of the same image ensures that the model treats images with the same subject matter the same, regardless of size. Mean Square Error (MSE) loss between the attention block outputs is designed to reinforce that relationship, and then standard reconstruction loss encourages learning intra-image semantics. OmniSat performs very well on the RESISC45 [28] task, which features images with varying spatial resolution, compared to other spatially aware models, such as ScaleMAE [100]. OmniSat explores adding the GSD embedding present in ScaleMAE and finds that it does not improve performance. The author's theorize that it provides redundant information,

and further point to the fact that incorporating GSD on SatMAE [32], which has no spatial awareness, improves performance.

Geospatial Foundation Model (GFM) [85] also leverages multiple approaches to train on a single sensor. Where Cross-Scale MAE focuses on understanding spatial resolution, GFM focuses on treating RS imagery as an extension of natural imagery, performing continual pre-training with models trained on the ubiquitous ImageNet [104] dataset. GFM draws inspiration from the fact that that MIM can trivialize the task when training on data with low entropy. In other words, if there is not much difference from patch to patch, then the network simply does not work as hard to reconstruct a masked patch. GFM calculates the average entropy of 3k randomly selected images from ImageNet and Sentinel-2 and find that Sentinel-2 images have an entropy of 3.9, compared to an entropy of 5.1 for ImageNet [85]. GFM develops a two-pronged learning approach to address this issue. GFM maintains a student encoder and teacher encoder, but the teacher encoder is an entirely frozen model initialized with weights from training on ImageNet. For each image, the student is fed a masked version of the image, and the teacher is fed an unmasked version. Then, there are two loss terms generated:

- the cosine similarity between the teacher and the student embeddings
- reconstruction loss from trying to reconstruct the original image through the student embeddings

This framework is designed to leverage pre-existing work in CV via distillation to minimize the overhead needed to train RS foundation models. Distilling against a pre-trained ImageNet model lets GFM quickly learn how to extract features from images, taking advantage of the higher entropy present in the ImageNet images. The additional MIM task ensures that GFM learns RS domain-specific information.

10 Future Considerations

Given the relative youth of foundation model development in RS, there is a high degree of fluidity in existing frameworks and overall goals.

10.1 Learning Representations in the Era of Climate Change

Given the rapidly shifting nature of the Earth’s climate, learned representations should be robust enough to take these changes into account without substantial retraining. Otherwise, the re-usability of these representations becomes less desirable and/or reliable over time, diminishing one of the main benefits of foundation models. When considering the variety of modalities present in RS, there is the potential to create representations that can withstand the challenges of a changing climate, but a degree of care is required. Relying too heavily on geographic locations and temporal data could very well result in representations that quickly become outdated as the world’s climate shifts. For example, a learned representation of a specific location on a coastline could cease to be relevant due to rising sea levels. Similarly, climate change has resulted in marked seasonal shifts within the past decade. Therefore, learning representations of what a given location looks like at a given time of year may wane in relevance as well.

By comparison, representations based on modalities that directly observe the Earth, such as satellite imagery and text, should be more tolerant to climate change-induced drift. Such representations are tied to understanding underlying observations directly within the data and are less reliant on climate context. Given that many remotely sensed datasets date back decades, there is merit in creating foundation models that perform time-series forecasting over long time periods in order to effectively learn representations which take long-term trends into account. This historical data also

opens the door for assessing the capability of RS foundation models to quantify historically understood climate and biome changes.

The combination of historical data and the steady incoming stream of satellite data from currently orbiting satellite offers intriguing possibilities for continual pre-training, an approach popularized in NLP [135]. Continual pre-training focuses on efficiently adapting existing models to emerging knowledge in a field while maintaining previously learned knowledge. Within the remote sensing domain, GFM [85] has begun to explore this approach. However, GFM does so by continually training a CV model against RS data, instead of continually training an existing RS model against a stream of new RS data. Developing a foundation model on historical data, and then performing continual pre-training against up-to-date RS data could prove useful for the development of climate change-tolerant RS foundation models. This approach may prove particularly pertinent when working with spatiotemporally dependent data modes, where the same scene may be re-contextualized due to climate change.

10.2 Under-Tapped Modes for Geospatial Representation Learning

Much of the current research focuses on drawing parallels to the work done on CV foundation models. Given the success of foundation models in the CV domain and the sheer amount of imagery that is available, be it from satellites or other aerial sources, this is a necessary first step. However, models such as MMCPP [26] use the CLIP contrastive learning objective and rely on other modalities, such as trajectory maps, points of interest, and aerial images. Their success should serve as a somewhat cautionary tale against becoming too invested in foundation models that purely focus on satellite and/or aerial imagery. Environmental stations measure features such as groundwater, weather, or snow melt data. They provide important climate and atmospheric information at a very high temporal resolution, often recording data on a daily or even hourly basis. More human-centric data, such as social media posts, social connectedness indices [8], and trajectory data, also provide invaluable information for understanding more societally-focused downstream tasks. Both forms of information are not observable from space, but could provide useful modes due to their different perspective and high temporal resolution. Data on rapidly changing phenomena also tends to not be observable from space. Changes can occur too quickly for a satellite to capture due to orbit and revisit time. GAIR's [76] usage of INR representations for satellite imagery also provides a useful starting point for mapping granular, ground-level data to satellite imagery.

10.3 Performance versus Training Expenses

Given the computational costs of training transformer models, the training expense of foundation models has rapidly become an obstacle across a variety of domains, with some models now including a section on carbon footprint [32]. As a substantial portion of downstream tasks for remote sensing pertain to combating the negative effects of climate change, there is a compelling argument for remote sensing foundation models to focus on curtailing training expenses. Massive models which create a large carbon footprint ultimately may be counterproductive from a climate change standpoint. However, the perpetual flow of remotely sensed data which dates back decades also encourages exploring the development of an incremental learning pipeline to efficiently fine-tune foundation models with up-to-date information.

Aside from a carbon footprint perspective, models with huge numbers of parameters have their downstream applications somewhat limited due to computational requirements. Not all users have the hardware necessary to fine-tune foundation models with a high parameter count. Some models, such as MOSAIKS [102], focus on lightweight frameworks in order to promote access to remote sensing foundation models. MOSAIKS has competitive results on a number of downstream tasks, indicating that increasing parameters within RS foundation models may follow a law

of diminishing returns. On the other hand, the encoder-decoder structure that is predominant in foundation models allows for repeated, diverse usage of representations on downstream tasks. Arguably, leveraging significant resources to generate high quality embeddings as a one-time cost is the most effective path moving forward, as this approach results in SOTA performance on downstream tasks with relatively few resources necessary for future fine-tuning.

Other domains have specifically studied how the factors of data size, number of parameters, and compute affect overall model performance [66]. NLP has established a principle that performance increases with an increase in any of those factors, providing that neither of the other two serve as a bottleneck [66]. However, such studies in CV for MIM have demonstrated that large-scale data is a requirement for scaling up compute and model parameters [132]. Moreover, MIM cannot benefit from increasing the data size if the model is not overfitting [132]. To the best of our knowledge, such studies do not exist for the remote sensing field. Authors in CV cite the semantic richness in text tokens compared to the redundancy of visual tokens as a significant motivator for their study [132]. It stands to reason that the significant differences in natural imagery and remotely sensed imagery would also motivate such a study in the remote sensing field.

It is possible that SSL distillation networks may provide a happy medium between the desire for high quality embeddings and lower computational requirements. While models such as RS-BYOL [59], DINO-MM [4], and SkySense [47] have demonstrated that such an approach is feasible with remotely sensed imagery, distillation has yet to be explored as a SSL approach in remote sensing to the degree that masked image modelling or contrastive learning with negative samples have been. The recent and well-publicized success of DeepSeek [129] in the NLP field also highlights the viability of distillation for knowledge compression and indicates that it should be further examined within the remote sensing domain. GFM [85] begins to inspect the efficacy of distilling knowledge from the CV domain into remote sensing, but there remains substantial room for exploration.

A Mixture of Experts (MoE) approach may also provide an intriguing compromise between embedding quality and computational requirements. At a high level, MoE partitions an input space into non-overlapping regions, then designates an 'expert' model per region [42]. This particular approach allows for flexible incorporation of models for a variety of modalities and tasks, yet remains computationally efficient since only a subset of experts are activated at training and inference. The Switch Transformer [39], an NLP model for multilingual learning, followed the MoE paradigm to develop a foundation model with over a trillion trainable parameters. In addition to the enormous parameter count, the Switch Transformer also trains significantly faster than comparable models on the same hardware [39]. The MoE framework's capabilities in efficiently leveraging mode and task specific models make it an exciting avenue for exploration in RS foundation models. To the best of our knowledge, a MoE-based remote sensing foundation model does not yet exist.

10.4 Directions for Framework Development

Many of the foundation models covered in this manuscript leverage a variety of different objectives that force the encoder to learn accurate representations of the data and test on downstream generalizability. Many of these models use a single pretext task training objective in the hopes of generating a general representation. In other domains, such as NLP, multiple pretext tasks are optimized simultaneously as a key part of learning generalizable embeddings [69]. RS foundation models could profit from a similar strategy.

MMEarth [89] utilizes multi-task training, as the model uses a variety of downstream decoders for different modalities that each backpropagate loss to the same encoder. FG-MAE [127] takes this a step further by tasking decoders to not just reconstruct a different modality, but to reconstruct specific RS feature maps pertaining to the masked training

image. While we have discussed some approaches designed to leverage contrastive loss between modes that also include MAE within a mode, this remains an under-explored avenue. CROMA [41] begins to explore this possibility in the RS domain by contrasting two independently masked images, but this is explored mainly for performance reasons, and the MAE objective is on multi-sensed image embeddings as opposed to MAE for each sensor. This approach may scale poorly with the addition of more sensors due to input size. Similarly, the nature of a MAE task shared with multiple modalities seems to align these sensors more closely, rendering it somewhat redundant to the contrastive task already being executed. DeCUR [123] provides an interesting alternative to such approaches. It leverages the same redundancy reduction task across modes and within modes, but the choice to set aside roughly 20% of the latent space dimensions for learning modality specific features seems to be a framework choice that other foundation models could benefit from. Similarly, the regularization term in VICReg [10] that enforces a degree of standard deviation within each dimension is worth exploring as an avenue to prevent embedding collapse.

Most multi-modal models in the RS domain only consider two to three sensors, but the sheer number of modes available means that it would be beneficial to have a model that is capable of scaling effectively to learn representations that capture a dynamic number of modes. MMEarth's innovation of having a decoder per mode is promising in that regard, but it runs into the problem of only learning embeddings for one sensor. While contrastive learning can theoretically be applied across a variety of modes, the cost of training a separate encoder per sensor could quickly result in resource challenges. For example, OmniSat [5] leverages MAE per mode and contrastive loss across three modes, but the contrastive framework would scale poorly with the addition of more modalities. Ultimately, a multi-modal framework that is capable of learning representations for multiple sensors without explicitly requiring that every mode has its own encoder would be ideal, but careful consideration is required to develop a framework that is both flexible and robust enough. One potential option would be following an ImageBind [45] approach, where one modality is the 'binding' modality that all other modalities are contrasted to. Treating spatiotemporal location as a binding modality for any remotely sensed data could be an interesting avenue to pursue. Such a framework would allow incorporation of pre-trained, sensor-specific encoders. The number of comparisons made would scale linearly with the number of additional modalities, as opposed to exponentially.

DOFA's [133] hypernetwork-inspired framework is promising in that regard due to its ability to handle a variety of different sensor inputs in pre-training, but it fails to take into account whether a wavelength is being actively sensed or passively sensed, which affects the nature of the imagery. Similarly, the various polarization of SAR acquisitions, even by the same sensor, can create further complications that go beyond wavelength: The C-band Sentinel-1 SAR images land areas in VH and VV mode, whereas it switches to HH and HV polarizations when over oceans (this is driven by the scientific and operational users' need to map sea ice, which is better detectable in these modes). DOFA also does not demonstrably test what we consider to be this framework's most interesting potential capability: the capacity to operate effectively on downstream tasks that rely on a sensor not found in the training dataset.

SeCo [84] and GASSL [6] demonstrated the value of utilizing temporal data in training, but cautioned that the learned representations were agnostic to seasonal changes. The seasonal contrastive objective could be helpful as an additional task, when taken into account with other pre-training tasks that take seasonal change into account. Ultimately, multi-task training on complementary tasks, such as this particular example, is somewhat costly, but it results in representations that learn the unique features inherent to each task while avoiding the problem of overfitting. Aside from the SeCo objective, SatMAE's [32] breakthrough in adding temporal information to the positional encoding of images could serve as a useful way to introduce temporal information into existing methods. However, caution should be taken to ensure that such encoders are robust enough to not be overly reliant on temporal information. ScaleMAE's

[100] novel approach of normalizing positional embeddings to account for image scale also seems to be a methodology that could be easily applied to other models within the field, presuming those models utilize a ViT framework. Similarly, Cross-Scale MAE's [115] focus on random crop and resize augmentations as a way to learn spatial resolution could be applied to other contrastive and distillation based frameworks.

11 Conclusion

In this paper we presented on a variety of SSL approaches currently utilized in RS foundation models. We traced these approaches back to their origins in the CV field to develop a better understanding of the current swathe of RS foundation models and potential paths for future development.

We examined:

- (1) Varying benefits and drawbacks of RS embeddings learned with different frameworks and SSL tasks.
- (2) Prospective options for lowering compute costs for training RS foundation models.
- (3) Inherent opportunities available for leveraging multi-sensory Earth observations to train RS foundation models on publicly available unlabeled data.

Acknowledgments

To the GeoHAI lab, for all of their ideas, support, and kindness.

References

- [1] Suleiman O. Alsweiss, Zorana Jelenak, Paul S. Chang, Jun Dong Park, and Patrick Meyers. 2015. Inter-calibration Results of the Advanced Microwave Scanning Radiometer-2 Over Ocean. *IEEE Journal of Selected Topics in Applied Earth Observations and Remote Sensing* 8, 9 (Sept. 2015), 4230–4238. <https://doi.org/10.1109/JSTARS.2014.2330980> Conference Name: IEEE Journal of Selected Topics in Applied Earth Observations and Remote Sensing.
- [2] Neal T. Anderson and Giovanni B. Marchisio. 2012. WorldView-2 and the evolution of the DigitalGlobe remote sensing satellite constellation: introductory paper for the special session on WorldView-2. In *Algorithms and Technologies for Multispectral, Hyperspectral, and Ultraspectral Imagery XVIII*, Vol. 8390. SPIE, 166–180. <https://doi.org/10.1117/12.919756>
- [3] D. M. Anisuzzaman, Jeffrey G. Malins, Paul A. Friedman, and Zachi I. Attia. 2025. Fine-Tuning Large Language Models for Specialized Use Cases. *Mayo Clinic Proceedings: Digital Health* 3, 1 (March 2025), 100184. <https://doi.org/10.1016/j.mcpdig.2024.11.005>
- [4] Mahmoud Assran, Quentin Duval, Ishan Misra, Piotr Bojanowski, Pascal Vincent, Michael Rabbat, Yann LeCun, and Nicolas Ballas. 2023. Self-Supervised Learning From Images With a Joint-Embedding Predictive Architecture. 15619–15629. https://openaccess.thecvf.com/content/CVPR2023/html/Assran_Self-Supervised_Learning_From_Images_With_a_Joint-Embedding_Predictive_Architecture_CVPR_2023_paper.html
- [5] Guillaume Astruc, Nicolas Gonthier, Clement Mallet, and Loic Landrieu. 2024. OmniSat: Self-Supervised Modality Fusion for Earth Observation. <https://doi.org/10.48550/arXiv.2404.08351> arXiv:2404.08351 [cs].
- [6] Kumar Ayush, Burak Uzkent, Chenlin Meng, Kumar Tanmay, Marshall Burke, David Lobell, and Stefano Ermon. 2021. Geography-Aware Self-Supervised Learning. 10181–10190. https://openaccess.thecvf.com/content/ICCV2021/html/Ayush_Geography-Aware_Self-Supervised_Learning_ICCV_2021_paper.html
- [7] Gerald Baier, Antonin Deschamps, Michael Schmitt, and Naoto Yokoya. 2020. GeoNRW. <https://doi.org/10.21227/S5XQ-B822>
- [8] Michael Bailey, Rachel Cao, Theresa Kuchler, Johannes Stroebel, and Arlene Wong. 2018. Social Connectedness: Measurement, Determinants, and Effects. *Journal of Economic Perspectives* 32, 3 (Aug. 2018), 259–280. <https://doi.org/10.1257/jep.32.3.259>
- [9] Hangbo Bao, Li Dong, Songhao Piao, and Furu Wei. 2022. BEiT: BERT Pre-Training of Image Transformers. <https://doi.org/10.48550/arXiv.2106.08254> arXiv:2106.08254 [cs].
- [10] Adrien Bardes, Jean Ponce, and Yann LeCun. 2022. VICReg: Variance-Invariance-Covariance Regularization for Self-Supervised Learning. <https://doi.org/10.48550/arXiv.2105.04906> arXiv:2105.04906 [cs].
- [11] Jan Barowski, Jochen Jebramcik, Jonas Wagner, Nils Pohl, and Ilona Rolfs. 2019. Spatial Identification of Dielectric Properties using Synthetic Aperture Radar. In *2019 IEEE MTT-S International Microwave Workshop Series on Advanced Materials and Processes for RF and THz Applications (IMWS-AMP)*, 139–141. <https://doi.org/10.1109/IMWS-AMP.2019.8880121>
- [12] Derrick Bonafilia, Beth Tellman, Tyler Anderson, and Erica Issenberg. 2020. Sen1Floods11: A Georeferenced Dataset to Train and Test Deep Learning Flood Algorithms for Sentinel-1. 210–211. https://openaccess.thecvf.com/content_CVPRW_2020/html/w11/Bonafilia_Sen1Floods11_A_Georeferenced_Dataset_to_Train_and_Test_Deep_Learning_CVPRW_2020_paper.html

- [13] Nikolaos Ioannis Bountos, Arthur Ouaknine, Ioannis Papoutsis, and David Rolnick. 2025. FoMo: Multi-Modal, Multi-Scale and Multi-Task Remote Sensing Foundation Models for Forest Monitoring. *Proceedings of the AAAI Conference on Artificial Intelligence* 39, 27 (April 2025), 27858–27868. <https://doi.org/10.1609/aaai.v39i27.35002>
- [14] Christopher F. Brown, Steven P. Brumby, Brookie Guzder-Williams, Tanya Birch, Samantha Brooks Hyde, Joseph Mazzariello, Wanda Czerwinski, Valerie J. Pasquarella, Robert Haertel, Simon Ilyushchenko, Kurt Schwehr, Mikaela Weisse, Fred Stolle, Craig Hanson, Oliver Guinan, Rebecca Moore, and Alexander M. Tait. 2022. Dynamic World, Near real-time global 10 m land use land cover mapping. *Scientific Data* 9, 1 (June 2022), 251. <https://doi.org/10.1038/s41597-022-01307-4>
- [15] William M. Brown and Leonard J. Porcello. 1969. An introduction to synthetic-aperture radar. *IEEE Spectrum* 6, 9 (Sept. 1969), 52–62. <https://doi.org/10.1109/MSPEC.1969.5213674> Conference Name: IEEE Spectrum.
- [16] P. Burt and E. Adelson. 1983. The Laplacian Pyramid as a Compact Image Code. *IEEE Transactions on Communications* 31, 4 (April 1983), 532–540. <https://doi.org/10.1109/TCOM.1983.1095851> Conference Name: IEEE Transactions on Communications.
- [17] John Canny. 1986. A Computational Approach to Edge Detection. *IEEE Transactions on Pattern Analysis and Machine Intelligence* PAMI-8, 6 (Nov. 1986), 679–698. <https://doi.org/10.1109/TPAMI.1986.4767851> Conference Name: IEEE Transactions on Pattern Analysis and Machine Intelligence.
- [18] Mathilde Caron, Hugo Touvron, Ishan Misra, Hervé Jégou, Julien Mairal, Piotr Bojanowski, and Armand Joulin. 2021. Emerging Properties in Self-Supervised Vision Transformers. <https://doi.org/10.48550/arXiv.2104.14294> arXiv:2104.14294 [cs].
- [19] Davide Castelletti, Gordon Farquharson, Craig Stringham, Michael Duersch, and Duncan Eddy. 2021. Capella Space First Operational SAR Satellite. In *2021 IEEE International Geoscience and Remote Sensing Symposium IGARSS*. 1483–1486. <https://doi.org/10.1109/IGARSS47720.2021.9554100> ISSN: 2153-7003.
- [20] Vicente Vivanco Cepeda, Gaurav Kumar Nayak, and Mubarak Shah. 2023. GeoCLIP: Clip-Inspired Alignment between Locations and Images for Effective Worldwide Geo-localization. <http://arxiv.org/abs/2309.16020> arXiv:2309.16020 [cs].
- [21] Bruce Chapman and Paul Rosen. 2024. Overview of NASA'S calibration and validation activities for the NISAR mission. In *EUSAR 2024; 15th European Conference on Synthetic Aperture Radar*. 1101–1103. <https://ieeexplore.ieee.org/abstract/document/10659495>
- [22] Vinod Kumar Chauhan, Jiandong Zhou, Ping Lu, Soheila Molaei, and David A. Clifton. 2024. A brief review of hypernetworks in deep learning. *Artificial Intelligence Review* 57, 9 (Sept. 2024), 1–29. <https://doi.org/10.1007/s10462-024-10862-8> Company: Springer Distributor: Springer Institution: Springer Label: Springer Number: 9 Publisher: Springer Netherlands.
- [23] Ting Chen, Simon Kornblith, Mohammad Norouzi, and Geoffrey Hinton. 2020. A Simple Framework for Contrastive Learning of Visual Representations. <http://arxiv.org/abs/2002.05709> arXiv:2002.05709 [cs, stat].
- [24] Xinlei Chen and Kaiming He. 2021. Exploring Simple Siamese Representation Learning. 15750–15758. https://openaccess.thecvf.com/content_CVPR2021/html/Chen_Exploring_Simple_Siamese_Representation_Learning_CVPR_2021_paper.html
- [25] Yile Chen, Weiming Huang, Kaiqi Zhao, Yue Jiang, and Gao Cong. 2024. Self-supervised Learning for Geospatial AI: A Survey. <https://doi.org/10.48550/arXiv.2408.12133> arXiv:2408.12133 [cs].
- [26] Y. Chen, X. S. Yu, and K. Qin. 2023. MMCPP: A MULTI-MODAL CONTRASTIVE PRE-TRAINING MODEL FOR PLACE REPRESENTATION BASED ON THE SPATIO-TEMPORAL FRAMEWORK. *ISPRS Annals of the Photogrammetry, Remote Sensing and Spatial Information Sciences* X-1-W1-2023 (Dec. 2023), 303–310. <https://doi.org/10.5194/isprs-annals-X-1-W1-2023-303-2023> Conference Name: ISPRS Geospatial Week 2023 - 2–7 September 2023, Cairo, Egypt Publisher: Copernicus GmbH.
- [27] Zhengyang Chen, Yao Qian, Bing Han, Yanmin Qian, and Michael Zeng. 2022. A comprehensive study on self-supervised distillation for speaker representation learning. <https://doi.org/10.48550/arXiv.2210.15936> arXiv:2210.15936 [cs].
- [28] Gong Cheng, Junwei Han, and Xiaoqiang Lu. 2017. Remote Sensing Image Scene Classification: Benchmark and State of the Art. *Proc. IEEE* 105, 10 (Oct. 2017), 1865–1883. <https://doi.org/10.1109/JPROC.2017.2675998> Conference Name: Proceedings of the IEEE.
- [29] Gordon Christie, Neil Fendley, James Wilson, and Ryan Mukherjee. 2018. Functional Map of the World. <https://doi.org/10.48550/arXiv.1711.07846> arXiv:1711.07846 [cs].
- [30] Carmen Cillero Castro, Jose Antonio Domínguez Gómez, Jordi Delgado Martín, Boris Alejandro Hinojo Sánchez, Jose Luis Cereijo Arango, Federico Andrés Cheda Tuya, and Ramon Díaz-Varela. 2020. An UAV and Satellite Multispectral Data Approach to Monitor Water Quality in Small Reservoirs. *Remote Sensing* 12, 9 (Jan. 2020), 1514. <https://doi.org/10.3390/rs12091514> Number: 9 Publisher: Multidisciplinary Digital Publishing Institute.
- [31] Martin Claverie, Junchang Ju, Jeffrey G. Masek, Jennifer L. Dungan, Eric F. Vermote, Jean-Claude Roger, Sergii V. Skakun, and Christopher Justice. 2018. The Harmonized Landsat and Sentinel-2 surface reflectance data set. *Remote Sensing of Environment* 219 (Dec. 2018), 145–161. <https://doi.org/10.1016/j.rse.2018.09.002>
- [32] Yezhen Cong, Samar Khanna, Chenlin Meng, Patrick Liu, Erik Rozi, Yutong He, Marshall Burke, David B. Lobell, and Stefano Ermon. 2023. SatMAE: Pre-training Transformers for Temporal and Multi-Spectral Satellite Imagery. <https://doi.org/10.48550/arXiv.2207.08051> arXiv:2207.08051 [cs].
- [33] N. Dalal and B. Triggs. 2005. Histograms of oriented gradients for human detection. In *2005 IEEE Computer Society Conference on Computer Vision and Pattern Recognition (CVPR'05)*, Vol. 1. 886–893 vol. 1. <https://doi.org/10.1109/CVPR.2005.177> ISSN: 1063-6919.
- [34] Rodrigo Caye Daudt, Bertr Le Saux, Alexandre Boulch, and Yann Gousseau. 2018. Urban Change Detection for Multispectral Earth Observation Using Convolutional Neural Networks. In *IGARSS 2018 - 2018 IEEE International Geoscience and Remote Sensing Symposium*. 2115–2118. <https://doi.org/10.1109/IGARSS.2018.8518015> ISSN: 2153-7003.

[35] Mostafa Dehghani, Josip Djolonga, Basil Mustafa, Piotr Padlewski, Jonathan Heek, Justin Gilmer, Andreas Steiner, Mathilde Caron, Robert Geirhos, Ibrahim Alabdulmohsin, Rodolphe Jenatton, Lucas Beyer, Michael Tschannen, Anurag Arnab, Xiao Wang, Carlos Riquelme, Matthias Minderer, Joan Puigcerver, Utku Evci, Manoj Kumar, Sjoerd van Steenkiste, Gamaleldin F. Elsayed, Aravindh Mahendran, Fisher Yu, Avital Oliver, Fantine Huot, Jasmijn Bastings, Mark Patrick Collier, Alexey Gritsenko, Vighnesh Birodkar, Cristina Vasconcelos, Yi Tay, Thomas Mensink, Alexander Kolesnikov, Filip Pavetić, Dustin Tran, Thomas Kipf, Mario Lučić, Xiaohua Zhai, Daniel Keysers, Jeremiah Harmsen, and Neil Houlsby. 2023. Scaling Vision Transformers to 22 Billion Parameters. <https://doi.org/10.48550/arXiv.2302.05442> arXiv:2302.05442 [cs].

[36] Jacob Devlin, Ming-Wei Chang, Kenton Lee, and Kristina Toutanova. 2019. BERT: Pre-training of Deep Bidirectional Transformers for Language Understanding. <https://doi.org/10.48550/arXiv.1810.04805> arXiv:1810.04805 [cs].

[37] Alexey Dosovitskiy, Lucas Beyer, Alexander Kolesnikov, Dirk Weissenborn, Xiaohua Zhai, Thomas Unterthiner, Mostafa Dehghani, Matthias Minderer, Georg Heigold, Sylvain Gelly, Jakob Uszkoreit, and Neil Houlsby. 2021. An Image is Worth 16x16 Words: Transformers for Image Recognition at Scale. <https://doi.org/10.48550/arXiv.2010.11929> arXiv:2010.11929 [cs].

[38] Dara Entekhabi, Eni G. Njoku, Peggy E. O'Neill, Kent H. Kellogg, Wade T. Crow, Wendy N. Edelstein, Jared K. Entin, Shawn D. Goodman, Thomas J. Jackson, Joel Johnson, John Kimball, Jeffrey R. Piepmeier, Randal D. Koster, Neil Martin, Kyle C. McDonald, Mahta Moghaddam, Susan Moran, Rolf Reichle, J. C. Shi, Michael W. Spencer, Samuel W. Thurman, Leung Tsang, and Jakob Van Zyl. 2010. The Soil Moisture Active Passive (SMAP) Mission. *Proc. IEEE* 98, 5 (May 2010), 704–716. <https://doi.org/10.1109/JPROC.2010.2043918> Conference Name: Proceedings of the IEEE.

[39] William Fedus, Barret Zoph, and Noam Shazeer. 2022. Switch Transformers: Scaling to Trillion Parameter Models with Simple and Efficient Sparsity. <https://doi.org/10.48550/arXiv.2101.03961> arXiv:2101.03961 [cs].

[40] Christoph Feichtenhofer, Haoqi Fan, Yanghao Li, and Kaiming He. 2022. Masked Autoencoders As Spatiotemporal Learners. *Advances in Neural Information Processing Systems* 35 (Dec. 2022), 35946–35958. https://proceedings.neurips.cc/paper_files/paper/2022/hash/e97d1081481a4017df96b51be31001d3-Abstract-Conference.html

[41] Anthony Fuller, Koreen Millard, and James R. Green. 2023. CROMA: Remote Sensing Representations with Contrastive Radar-Optical Masked Autoencoders. <https://doi.org/10.48550/arXiv.2311.00566> arXiv:2311.00566 [cs].

[42] Fawzi Gamal, Tariq Afifa, and Fawzi Gamal. 2025. MoE at Scale: From Modular Design to Deployment in Large-Scale Machine Learning Systems. <https://doi.org/10.20944/preprints202504.1313.v1>

[43] Guangshuai Gao, Qingjie Liu, and Yunhong Wang. 2021. Counting From Sky: A Large-Scale Data Set for Remote Sensing Object Counting and a Benchmark Method. *IEEE Transactions on Geoscience and Remote Sensing* 59, 5 (May 2021), 3642–3655. <https://doi.org/10.1109/TGRS.2020.3020555> Conference Name: IEEE Transactions on Geoscience and Remote Sensing.

[44] Tianyu Gao, Xingcheng Yao, and Danqi Chen. 2022. SimCSE: Simple Contrastive Learning of Sentence Embeddings. <https://doi.org/10.48550/arXiv.2104.08821> arXiv:2104.08821 [cs].

[45] Rohit Girdhar, Alaaeldin El-Nouby, Zhuang Liu, Mannat Singh, Kalyan Vasudev Alwala, Armand Joulin, and Ishan Misra. 2023. ImageBind: One Embedding Space To Bind Them All. <https://doi.org/10.48550/arXiv.2305.05665> arXiv:2305.05665 [cs].

[46] Jean-Bastien Grill, Florian Strub, Florent Altché, Corentin Tallec, Pierre H. Richemond, Elena Buchatskaya, Carl Doersch, Bernardo Avila Pires, Zhaohan Daniel Guo, Mohammad Gheshlaghi Azar, Bilal Piot, Koray Kavukcuoglu, Rémi Munos, and Michal Valko. 2020. Bootstrap your own latent: A new approach to self-supervised Learning. <https://doi.org/10.48550/arXiv.2006.07733> arXiv:2006.07733 [cs, stat].

[47] Xin Guo, Jiangwei Lao, Bo Dang, Yingying Zhang, Lei Yu, Lixiang Ru, Liheng Zhong, Ziyuan Huang, Kang Wu, Dingxiang Hu, Huimei He, Jian Wang, Jingdong Chen, Ming Yang, Yongjun Zhang, and Yansheng Li. 2024. SkySense: A Multi-Modal Remote Sensing Foundation Model Towards Universal Interpretation for Earth Observation Imagery. In *2024 IEEE/CVF Conference on Computer Vision and Pattern Recognition (CVPR)*. IEEE, Seattle, WA, USA, 27662–27673. <https://doi.org/10.1109/CVPR52733.2024.02613>

[48] Dipanwita Halder, Anup Das, Shiv Mohan, Om Pal, Ramesh S. Hooda, and Manab Chakraborty. 2012. ASSESSMENT OF L-BAND SAR DATA AT DIFFERENT POLARIZATION COMBINATIONS FOR CROP AND OTHER LANDUSE CLASSIFICATION. *Progress In Electromagnetics Research B* 36 (2012), 303–321. <https://doi.org/10.2528/PIERB11071106>

[49] Kaiming He, Xinlei Chen, Saining Xie, Yanghao Li, Piotr Dollár, and Ross Girshick. 2021. Masked Autoencoders Are Scalable Vision Learners. <https://doi.org/10.48550/arXiv.2111.06377> arXiv:2111.06377 [cs].

[50] Kaiming He, Haoqi Fan, Yuxin Wu, Saining Xie, and Ross Girshick. 2020. Momentum Contrast for Unsupervised Visual Representation Learning. 9729–9738. https://openaccess.thecvf.com/content_CVPR_2020/html/He_Momentum_Contrast_for_Unsupervised_Visual_Representation_Learning_CVPR_2020_paper.html

[51] Kaiming He, Xiangyu Zhang, Shaoqing Ren, and Jian Sun. 2015. Deep Residual Learning for Image Recognition. <https://doi.org/10.48550/arXiv.1512.03385> arXiv:1512.03385 [cs].

[52] Patrick Helber, Benjamin Bischke, Andreas Dengel, and Damian Borth. 2019. EuroSAT: A Novel Dataset and Deep Learning Benchmark for Land Use and Land Cover Classification. <https://doi.org/10.48550/arXiv.1709.00029> arXiv:1709.00029 version: 2.

[53] D. H. Hoekman and B. A. M. Bouman. 1993. Interpretation of C- and X-band radar images over an agricultural area, the Flevoland test site in the Agriscatt-87 campaign. *International Journal of Remote Sensing* 14, 8 (May 1993), 1577–1594. <https://doi.org/10.1080/01431169308953987>

[54] Danfeng Hong, Bing Zhang, Xuyang Li, Yuxuan Li, Chenyu Li, Jing Yao, Naoto Yokoya, Hao Li, Pedram Ghamisi, Xiuping Jia, Antonio Plaza, Paolo Gamba, Jon Atli Benediktsson, and Jocelyn Chanussot. 2024. SpectralGPT: Spectral Remote Sensing Foundation Model. *IEEE Transactions on Pattern Analysis and Machine Intelligence* 46, 8 (Aug. 2024), 5227–5244. <https://doi.org/10.1109/TPAMI.2024.3362475> Conference Name: IEEE Transactions on Pattern Analysis and Machine Intelligence.

[55] Yujun Hou, Matias Quintana, Maxim Khomiakov, Winston Yap, Jian Ouyang, Koichi Ito, Zeyu Wang, Tianhong Zhao, and Filip Biljecki. 2024. Global Streetscapes – A comprehensive dataset of 10 million street-level images across 688 cities for urban science and analytics. *ISPRS Journal of Photogrammetry and Remote Sensing* 215 (Sept. 2024), 216–238. <https://doi.org/10.1016/j.isprsjprs.2024.06.023>

[56] Sha Huang, Lina Tang, Joseph P. Hupy, Yang Wang, and Guofan Shao. 2021. A commentary review on the use of normalized difference vegetation index (NDVI) in the era of popular remote sensing. *Journal of Forestry Research* 32, 1 (Feb. 2021), 1–6. <https://doi.org/10.1007/s11676-020-01155-1>

[57] Vladimir Ignatenko, Pekka Laurila, Andrea Radius, Leszek Lamentowski, Oleg Antropov, and Darren Muff. 2020. ICEYE Microsatellite SAR Constellation Status Update: Evaluation of First Commercial Imaging Modes. In *IGARSS 2020 - 2020 IEEE International Geoscience and Remote Sensing Symposium*. 3581–3584. <https://doi.org/10.1109/IGARSS39084.2020.9324531> ISSN: 2153-7003.

[58] Jeremy Irvin, Lucas Tao, Joanne Zhou, Yuntao Ma, Langston Nashold, Benjamin Liu, and Andrew Y. Ng. 2023. USat: A Unified Self-Supervised Encoder for Multi-Sensor Satellite Imagery. <https://doi.org/10.48550/arXiv.2312.02199> arXiv:2312.02199 [cs].

[59] Pallavi Jain, Bianca Schoen-Phelan, and Robert Ross. 2022. Self-Supervised Learning for Invariant Representations from Multi-Spectral and SAR Images. *IEEE Journal of Selected Topics in Applied Earth Observations and Remote Sensing* 15 (2022), 7797–7808. <https://doi.org/10.1109/JSTARS.2022.3204888> arXiv:2205.02049 [cs].

[60] Umangi Jain, Alex Wilson, and Varun Gulshan. 2022. Multimodal contrastive learning for remote sensing tasks. <http://arxiv.org/abs/2209.02329> arXiv:2209.02329 [cs].

[61] Johannes Jakubik, Sujit Roy, C. E. Phillips, Paolo Fraccaro, Denys Godwin, Bianca Zadrozny, Daniela Szwarcman, Carlos Gomes, Gabby Nyirjesy, Blair Edwards, Daiki Kimura, Naomi Simumba, Linsong Chu, S. Karthik Mukkavilli, Devyani Lambhate, Kamal Das, Ranjini Bangalore, Dario Oliveira, Michal Muszynski, Kumar Ankur, Muthukumaran Ramasubramanian, Iksha Gurung, Sam Khallaghi, Hanxi Li, Michael Cecil, Maryam Ahmadi, Fatemeh Kordi, Hamed Alemohammad, Manil Maskey, Raghu Ganti, Kommy Weldemariam, and Rahul Ramachandran. 2023. Foundation Models for Generalist Geospatial Artificial Intelligence. <http://arxiv.org/abs/2310.18660> arXiv:2310.18660 [cs].

[62] Jiho Jang, Seonhoon Kim, Kiyoon Yoo, Chaerin Kong, Jangho Kim, and Nojun Kwak. 2023. Self-Distilled Self-supervised Representation Learning. In *2023 IEEE/CVF Winter Conference on Applications of Computer Vision (WACV)*. IEEE, Waikoloa, HI, USA, 2828–2838. <https://doi.org/10.1109/WACV56688.2023.00285>

[63] Chao Jia, Yinfei Yang, Ye Xia, Yi-Ting Chen, Zarana Parekh, Hieu Pham, Quoc V. Le, Yunhsuan Sung, Zhen Li, and Tom Duerig. 2021. Scaling Up Visual and Vision-Language Representation Learning With Noisy Text Supervision. <https://doi.org/10.48550/arXiv.2102.05918> arXiv:2102.05918 [cs].

[64] Li Jing, Pascal Vincent, Yann LeCun, and Yuandong Tian. 2022. Understanding Dimensional Collapse in Contrastive Self-supervised Learning. <https://doi.org/10.48550/arXiv.2110.09348> arXiv:2110.09348.

[65] C. O Justice, J. R. G Townshend, E. F Vermote, E Masuoka, R. E Wolfe, N Saleous, D. P Roy, and J. T Morisette. 2002. An overview of MODIS Land data processing and product status. *Remote Sensing of Environment* 83, 1 (Nov. 2002), 3–15. [https://doi.org/10.1016/S0034-4257\(02\)00084-6](https://doi.org/10.1016/S0034-4257(02)00084-6)

[66] Jared Kaplan, Sam McCandlish, Tom Henighan, Tom B. Brown, Benjamin Chess, Rewon Child, Scott Gray, Alec Radford, Jeffrey Wu, and Dario Amodei. 2020. Scaling Laws for Neural Language Models. <https://doi.org/10.48550/arXiv.2001.08361> arXiv:2001.08361 [cs].

[67] Konstantin Klemmer, Esther Rolf, Caleb Robinson, Lester Mackey, and Marc Rufwurm. 2024. SatCLIP: Global, General-Purpose Location Embeddings with Satellite Imagery. <https://doi.org/10.48550/arXiv.2311.17179> arXiv:2311.17179 [cs].

[68] Philip A. Knight. 2008. The Sinkhorn–Knopp Algorithm: Convergence and Applications. *SIAM J. Matrix Anal. Appl.* 30, 1 (Jan. 2008), 261–275. <https://doi.org/10.1137/060659624> Publisher: Society for Industrial and Applied Mathematics.

[69] M. V. Koroteev. 2021. BERT: A Review of Applications in Natural Language Processing and Understanding. <https://doi.org/10.48550/arXiv.2103.11943> arXiv:2103.11943 [cs].

[70] Gerhard Krieger, Alberto Moreira, Hauke Fiedler, Irena Hajnsek, Marian Werner, Marwan Younis, and Manfred Zink. 2007. TanDEM-X: A Satellite Formation for High-Resolution SAR Interferometry. *IEEE Transactions on Geoscience and Remote Sensing* 45, 11 (Nov. 2007), 3317–3341. <https://doi.org/10.1109/TGRS.2007.900693>

[71] Alexandre Lacoste, Nils Lehmann, Pau Rodriguez, Evan David Sherwin, Hannah Kerner, Björn Lütjens, Jeremy Andrew Irvin, David Dao, Hamed Alemohammad, Alexandre Drouin, Mehmet Gunturkun, Gabriel Huang, David Vazquez, Dava Newman, Yoshua Bengio, Stefano Ermon, and Xiao Xiang Zhu. 2023. GEO-Bench: Toward Foundation Models for Earth Monitoring. <http://arxiv.org/abs/2306.03831> arXiv:2306.03831 [cs].

[72] Liunian Harold Li, Mark Yatskar, Da Yin, Cho-Jui Hsieh, and Kai-Wei Chang. 2019. VisualBERT: A Simple and Performant Baseline for Vision and Language. <https://doi.org/10.48550/arXiv.1908.03557> arXiv:1908.03557 [cs].

[73] Xuyang Li, Danfeng Hong, and Jocelyn Chanussot. 2024. S2MAE: A Spatial-Spectral Pretraining Foundation Model for Spectral Remote Sensing Data. In *2024 IEEE/CVF Conference on Computer Vision and Pattern Recognition (CVPR)*. IEEE, Seattle, WA, USA, 27696–27705. <https://doi.org/10.1109/CVPR52733.2024.02616>

[74] Zhihao Li, Biao Hou, Siteng Ma, Zitong Wu, Xianpeng Guo, Bo Ren, and Licheng Jiao. 2024. Masked Angle-Aware Autoencoder for Remote Sensing Images. <https://doi.org/10.48550/arXiv.2408.01946> arXiv:2408.01946 [cs].

[75] Fan Liu, Delong Chen, Zhangqinyun Guan, Xiaocong Zhou, Jiale Zhu, Qiaolin Ye, Liyong Fu, and Jun Zhou. 2024. RemoteCLIP: A Vision Language Foundation Model for Remote Sensing. *IEEE Transactions on Geoscience and Remote Sensing* 62 (2024), 1–16. <https://doi.org/10.1109/TGRS.2024.3390838> Conference Name: IEEE Transactions on Geoscience and Remote Sensing.

[76] Zeping Liu, Fan Zhang, Junfeng Jiao, Ni Lao, and Gengchen Mai. 2025. GAIR: Improving Multimodal Geo-Foundation Model with Geo-Aligned Implicit Representations. <https://doi.org/10.48550/arXiv.2503.16683> arXiv:2503.16683 [cs].

[77] Yang Long, Gui-Song Xia, Shengyang Li, Wen Yang, Michael Ying Yang, Xiao Xiang Zhu, Liangpei Zhang, and Deren Li. 2021. On Creating Benchmark Dataset for Aerial Image Interpretation: Reviews, Guidances, and Million-AID. *IEEE Journal of Selected Topics in Applied Earth Observations and Remote Sensing* 14 (2021), 4205–4230. <https://doi.org/10.1109/JSTARS.2021.3070368> Conference Name: IEEE Journal of Selected Topics in Applied Earth Observations and Remote Sensing.

[78] David G. Lowe. 2004. Distinctive Image Features from Scale-Invariant Keypoints. *International Journal of Computer Vision* 60, 2 (Nov. 2004), 91–110. <https://doi.org/10.1023/B:VISI.0000029664.99615.94>

[79] Jiasen Lu, Dhruv Batra, Devi Parikh, and Stefan Lee. 2019. ViLBERT: Pretraining Task-Agnostic Visiolinguistic Representations for Vision-and-Language Tasks. In *Advances in Neural Information Processing Systems*, Vol. 32. Curran Associates, Inc. https://proceedings.neurips.cc/paper_files/paper/2019/hash/c74d97b01eae257e44aa9d5bade97baf-Abstract.html

[80] Siqi Lu, Junlin Guo, James R. Zimmer-Dauphinee, Jordan M. Nieuwsma, Xiao Wang, Parker VanValkenburgh, Steven A. Wernke, and Yuankai Huo. 2025. Vision Foundation Models in Remote Sensing: A Survey. <https://doi.org/10.48550/arXiv.2408.03464> arXiv:2408.03464 [cs].

[81] Ahmed Mahmood. 2014. RADARSAT-1 Background Mission Implementation and Accomplishments. *Canadian Journal of Remote Sensing* 40, 6 (Nov. 2014), 385–395. <https://doi.org/10.1080/07038992.2014.999913> Publisher: Canadian Aeronautics and Space Institute _eprint: <https://doi.org/10.1080/07038992.2014.999913>

[82] Gengchen Mai, Weiming Huang, Jin Sun, Suhang Song, Deepak Mishra, Ninghao Liu, Song Gao, Tianming Liu, Gao Cong, Yingjie Hu, Chris Cundy, Ziyuan Li, Rui Zhu, and Ni Lao. 2023. On the Opportunities and Challenges of Foundation Models for Geospatial Artificial Intelligence. <https://doi.org/10.48550/arXiv.2304.06798> arXiv:2304.06798 [cs].

[83] Gengchen Mai, Ni Lao, Yutong He, Jiaming Song, and Stefano Ermon. 2023. CSP: Self-Supervised Contrastive Spatial Pre-Training for Geospatial-Visual Representations. <http://arxiv.org/abs/2305.01118> arXiv:2305.01118.

[84] Oscar Mañas, Alexandre Lacoste, Xavier Giro-i Nieto, David Vazquez, and Pau Rodriguez. 2021. Seasonal Contrast: Unsupervised Pre-Training from Uncurated Remote Sensing Data. <https://doi.org/10.48550/arXiv.2103.16607> arXiv:2103.16607 [cs].

[85] Matias Mendieta, Boran Han, Xingjian Shi, Yi Zhu, and Chen Chen. 2023. Towards Geospatial Foundation Models via Continual Pretraining. <https://doi.org/10.48550/arXiv.2302.04476> arXiv:2302.04476 [cs].

[86] Harvey J. Miller. 2004. Tobler's First Law and Spatial Analysis. *Annals of the Association of American Geographers* 94, 2 (June 2004), 284–289. <https://doi.org/10.1111/j.1467-8306.2004.09402005.x> Publisher: Routledge _eprint: <https://doi.org/10.1111/j.1467-8306.2004.09402005.x>

[87] L C Morena, James , K V, , and J. Beck. 2004. An introduction to the RADARSAT-2 mission. *Canadian Journal of Remote Sensing* 30, 3 (Jan. 2004), 221–234. <https://doi.org/10.5589/m04-004> Publisher: Canadian Aeronautics and Space Institute _eprint: <https://doi.org/10.5589/m04-004>

[88] S. Joseph Munchak, Sarah Ringerud, Ludovic Brucker, Yalei You, Iris de Gelis, and Catherine Prigent. 2020. An Active–Passive Microwave Land Surface Database From GPM. *IEEE Transactions on Geoscience and Remote Sensing* 58, 9 (Sept. 2020), 6224–6242. <https://doi.org/10.1109/TGRS.2020.2975477> Conference Name: IEEE Transactions on Geoscience and Remote Sensing.

[89] Vishal Nedungadi, Ankit Kariryaa, Stefan Oehmcke, Serge Belongie, Christian Igel, and Nico Lang. 2024. MMEarth: Exploring Multi-Modal Pretext Tasks For Geospatial Representation Learning. <http://arxiv.org/abs/2405.02771> arXiv:2405.02771 [cs].

[90] Elnaz Neinavaz, Martin Schlerf, Roshanak Darvishzadeh, Max Gerhards, and Andrew K. Skidmore. 2021. Thermal infrared remote sensing of vegetation: Current status and perspectives. *International Journal of Applied Earth Observation and Geoinformation* 102 (Oct. 2021), 102415. <https://doi.org/10.1016/j.jag.2021.102415>

[91] Mubashir Noman, Muzammal Naseer, Hisham Cholakkal, Rao Muhammad Anwar, Salman Khan, and Fahad Shahbaz Khan. 2024. Rethinking Transformers Pre-training for Multi-Spectral Satellite Imagery. <https://doi.org/10.48550/arXiv.2403.05419> arXiv:2403.05419 [cs].

[92] OpenAI, Josh Achiam, Steven Adler, Sandhini Agarwal, Lama Ahmad, Ilge Akkaya, Florencia Leoni Aleman, Diogo Almeida, Janko Altenschmidt, Sam Altman, Shyamal Anadkat, Red Avila, Igor Babuschkin, Suchir Balaji, Valerie Balcom, Paul Baltescu, Haiming Bao, Mohammad Bavarian, Jeff Belgum, Irwan Bello, Jake Berdine, Gabriel Bernadett-Shapiro, Christopher Berner, Lenny Bogdonoff, Oleg Boiko, Madelaine Boyd, Anna-Luisa Brakman, Greg Brockman, Tim Brooks, Miles Brundage, Kevin Button, Trevor Cai, Rosie Campbell, Andrew Cann, Brittany Carey, Chelsea Carlson, Rory Carmichael, Brooke Chan, Che Chang, Fotis Chantzis, Derek Chen, Sully Chen, Ruby Chen, Jason Chen, Mark Chen, Ben Chess, Chester Cho, Casey Chu, Hyung Won Chung, Dave Cummings, Jeremiah Currier, Yunxing Dai, Cory Decareaux, Thomas Degry, Noah Deutsch, Damien Deville, Arka Dhar, David Dohan, Steve Dowling, Sheila Dunning, Adrien Ecoffet, Atty Eleti, Tyna Eloundou, David Farhi, Liam Fedus, Niko Felix, Simón Posada Fishman, Juston Forte, Isabella Fulford, Leo Gao, Elie Georges, Christian Gibson, Vik Goel, Tarun Gogineni, Gabriel Goh, Rapha Gontijo-Lopes, Jonathan Gordon, Morgan Grafstein, Scott Gray, Ryan Greene, Joshua Gross, Shixiang Shane Gu, Yufei Guo, Chris Hallacy, Jesse Han, Jeff Harris, Yuchen He, Mike Heaton, Johannes Heidecke, Chris Hesse, Alan Hickey, Wade Hickey, Peter Hoeschele, Brandon Houghton, Kenny Hsu, Shengli Hu, Xin Hu, Joost Huizinga, Shantanu Jain, Shawn Jain, Joanne Jang, Angela Jiang, Roger Jiang, Haozun Jin, Denny Jin, Shino Jomoto, Billie Jonn, Heewoo Jun, Tomer Kaftan, Łukasz Kaiser, Ali Kamali, Ingmar Kanitscheider, Nitish Shirish Keskar, Tabarak Khan, Logan Kilpatrick, Jong Wook Kim, Christina Kim, Yongjik Kim, Jan Hendrik Kirchner, Jamie Kiros, Matt Knight, Daniel Kokotajlo, Łukasz Kondraciuk, Andrew Kondrich, Aris Konstantinidis, Kyle Kosic, Gretchen Krueger, Vishal Kuo, Michael Lampe, Ikai Lan, Teddy Lee, Jan Leike, Jade Leung, Daniel Levy, Chak Ming Li, Rachel Lim, Molly Lin, Stephanie Lin, Mateusz Litwin, Theresa Lopez, Ryan Lowe, Patricia Lue, Anna Makanju, Kim Malfacini, Sam Manning, Todor Markov, Yaniv Markovski, Bianca Martin, Katie Mayer, Andrew Mayne, Bob McGrew, Scott Mayer McKinney, Christine McLeavey, Paul McMillan, Jake McNeil, David Medina, Aalok Mehta, Jacob Menick, Luke Metz, Andrey Mishchenko, Pamela Mishkin, Vinnie Monaco, Evan Morikawa, Daniel Mossing, Tong Mu, Mira Murati, Oleg Murk, David Mély, Ashvin Nair, Reiichiro Nakano, Rajeev Nayak, Arvind Neelakantan, Richard Ngo, Hyeonwoo Noh, Long Ouyang, Cullen O'Keefe, Jakub Pachocki, Alex Paino, Joe Palermo, Ashley Pantuliano,

Giambattista Parascandolo, Joel Parish, Emy Parparita, Alex Passos, Mikhail Pavlov, Andrew Peng, Adam Perelman, Filipe de Avila Belbute Peres, Michael Petrov, Henrique Ponde de Oliveira Pinto, Michael, Pokorny, Michelle Pokrass, Vitchyr H. Pong, Tolly Powell, Alethea Power, Boris Power, Elizabeth Proehl, Raul Puri, Alec Radford, Jack Rae, Aditya Ramesh, Cameron Raymond, Francis Real, Kendra Rimbach, Carl Ross, Bob Rotsted, Henri Roussez, Nick Ryder, Mario Saltarelli, Ted Sanders, Shibani Santurkar, Girish Sastry, Heather Schmidt, David Schnurr, John Schulman, Daniel Selsam, Kyla Sheppard, Toki Sherbakov, Jessica Shieh, Sarah Shoker, Pranav Shyam, Szymon Sidor, Eric Sigler, Maddie Simens, Jordan Sitkin, Katarina Slama, Ian Sohl, Benjamin Sokolowsky, Yang Song, Natalie Staudacher, Felipe Petroski Such, Natalie Summers, Ilya Sutskever, Jie Tang, Nikolas Tezak, Madeleine B. Thompson, Phil Tillet, Amin Tootoonchian, Elizabeth Tseng, Preston Tuggle, Nick Turley, Jerry Tworek, Juan Felipe Cerón Uribe, Andrea Vallone, Arun Vijayvergiya, Chelsea Voss, Carroll Wainwright, Justin Jay Wang, Alvin Wang, Ben Wang, Jonathan Ward, Jason Wei, C. J. Weinmann, Akila Welihinda, Peter Welinder, Jiayi Weng, Lilian Weng, Matt Wiethoff, Dave Willner, Clemens Winter, Samuel Wolrich, Hannah Wong, Lauren Workman, Sherwin Wu, Jeff Wu, Michael Wu, Kai Xiao, Tao Xu, Sarah Yoo, Kevin Yu, Qiming Yuan, Wojciech Zaremba, Rowan Zellers, Chong Zhang, Marvin Zhang, Shengjia Zhao, Tianhao Zheng, Juntang Zhuang, William Zhuk, and Barret Zoph. 2024. GPT-4 Technical Report. <https://doi.org/10.48550/arXiv.2303.08774> arXiv:2303.08774 [cs].

[93] Maxime Oquab, Timothée Darct, Théo Moutakanni, Huy Vo, Marc Szafraniec, Vasil Khalidov, Pierre Fernandez, Daniel Haziza, Francisco Massa, Alaeldin El-Nouby, Mahmoud Assran, Nicolas Ballas, Wojciech Galuba, Russell Howes, Po-Yao Huang, Shang-Wen Li, Ishan Misra, Michael Rabbat, Vasu Sharma, Gabriel Synnaeve, Hu Xu, Hervé Jegou, Julien Mairal, Patrick Labatut, Armand Joulin, and Piotr Bojanowski. 2024. DINOV2: Learning Robust Visual Features without Supervision. <https://doi.org/10.48550/arXiv.2304.07193> arXiv:2304.07193 [cs].

[94] Mary Phuong and Christoph Lampert. 2019. Towards Understanding Knowledge Distillation. In *Proceedings of the 36th International Conference on Machine Learning*. PMLR, 5142–5151. <https://proceedings.mlr.press/v97/phuong19a.html> ISSN: 2640-3498.

[95] Rafael Pires de Lima, Behzad Vahedi, Nick Hughes, Andrew P. Barrett, Walter Meier, and Morteza Karimzadeh. 2023. Enhancing sea ice segmentation in Sentinel-1 images with atrous convolutions. *International Journal of Remote Sensing* 44, 17 (Sept. 2023), 5344–5374. <https://doi.org/10.1080/01431161.2023.2248560> Publisher: Taylor & Francis _eprint: <https://doi.org/10.1080/01431161.2023.2248560>.

[96] Dimitris Poursanidis, Dimosthenis Traganos, Peter Reinartz, and Nektarios Chrysoulakis. 2019. On the use of Sentinel-2 for coastal habitat mapping and satellite-derived bathymetry estimation using downscaled coastal aerosol band. *International Journal of Applied Earth Observation and Geoinformation* 80 (Aug. 2019), 58–70. <https://doi.org/10.1016/j.jag.2019.03.012>

[97] Ofir Press, Noah A. Smith, and Mike Lewis. 2022. Train Short, Test Long: Attention with Linear Biases Enables Input Length Extrapolation. <https://doi.org/10.48550/arXiv.2108.12409> arXiv:2108.12409 [cs].

[98] Alec Radford, Jong Wook Kim, Chris Hallacy, Aditya Ramesh, Gabriel Goh, Sandhini Agarwal, Girish Sastry, Amanda Askell, Pamela Mishkin, Jack Clark, Gretchen Krueger, and Ilya Sutskever. 2021. Learning Transferable Visual Models From Natural Language Supervision. <http://arxiv.org/abs/2103.00020> arXiv:2103.00020 [cs].

[99] Alec Radford, Jeffrey Wu, Rewon Child, David Luan, Dario Amodei, and Ilya Sutskever. [n. d.]. Language Models are Unsupervised Multitask Learners. ([n. d.]).

[100] Colorado J. Reed, Ritwik Gupta, Shufan Li, Sarah Brockman, Christopher Funk, Brian Clipp, Kurt Keutzer, Salvatore Candido, Matt Uyttendaele, and Trevor Darrell. 2023. Scale-MAE: A Scale-Aware Masked Autoencoder for Multiscale Geospatial Representation Learning. <https://doi.org/10.48550/arXiv.2212.14532> arXiv:2212.14532 [cs].

[101] Esther Rolf, Konstantin Klemmer, Caleb Robinson, and Hannah Kerner. 2024. Mission Critical – Satellite Data is a Distinct Modality in Machine Learning. <https://doi.org/10.48550/arXiv.2402.01444> arXiv:2402.01444 [cs].

[102] Esther Rolf, Jonathan Proctor, Tamara Carleton, Ian Bolliger, Vaishaal Shankar, Miyabi Ishihara, Benjamin Recht, and Solomon Hsiang. 2021. A generalizable and accessible approach to machine learning with global satellite imagery. *Nature Communications* 12, 1 (July 2021), 4392. <https://doi.org/10.1038/s41467-021-24638-z>

[103] Ake Rosenqvist, Masanobu Shimada, Norimasa Ito, and Manabu Watanabe. 2007. ALOS PALSAR: A Pathfinder Mission for Global-Scale Monitoring of the Environment. *IEEE Transactions on Geoscience and Remote Sensing* 45, 11 (Nov. 2007), 3307–3316. <https://doi.org/10.1109/TGRS.2007.901027> Conference Name: IEEE Transactions on Geoscience and Remote Sensing.

[104] Olga Russakovsky, Jia Deng, Hao Su, Jonathan Krause, Sanjeev Satheesh, Sean Ma, Zhiheng Huang, Andrej Karpathy, Aditya Khosla, Michael Bernstein, Alexander C. Berg, and Li Fei-Fei. 2015. ImageNet Large Scale Visual Recognition Challenge. *International Journal of Computer Vision* 115, 3 (Dec. 2015), 211–252. <https://doi.org/10.1007/s11263-015-0816-y>

[105] Marc Rüßwurm, Konstantin Klemmer, Esther Rolf, Robin Zbinden, and Devis Tuia. 2024. Geographic Location Encoding with Spherical Harmonics and Sinusoidal Representation Networks. <http://arxiv.org/abs/2310.06743> arXiv:2310.06743 [cs].

[106] Amanpreet Singh, Ronghang Hu, Vedanuj Goswami, Guillaume Couairon, Wojciech Galuba, Marcus Rohrbach, and Douwe Kiela. 2022. FLAVA: A Foundational Language And Vision Alignment Model. In *2022 IEEE/CVF Conference on Computer Vision and Pattern Recognition (CVPR)*. IEEE, New Orleans, LA, USA, 15617–15629. <https://doi.org/10.1109/CVPR52688.2022.01519>

[107] Vincent Sitzmann, Julien N. P. Martel, Alexander W. Bergman, David B. Lindell, and Gordon Wetzstein. 2020. Implicit Neural Representations with Periodic Activation Functions. <https://doi.org/10.48550/arXiv.2006.09661> arXiv:2006.09661 [cs].

[108] Lorenzo Solaro, Andrea Ciampalini, Federico Raspini, Silvia Bianchini, Ivana Zinno, Manuela Bonano, Michele Manunta, Sandro Moretti, and Nicola Casagli. 2017. Combined Use of C- and X-Band SAR Data for Subsidence Monitoring in an Urban Area. *Geosciences* 7, 2 (June 2017), 21. <https://doi.org/10.3390/geosciences7020021> Number: 2 Publisher: Multidisciplinary Digital Publishing Institute.

[109] Shuran Song, Samuel P. Lichtenberg, and Jianxiong Xiao. 2015. SUN RGB-D: A RGB-D Scene Understanding Benchmark Suite. 567–576. https://openaccess.thecvf.com/content_cvpr_2015/html/Song_SUN_RGB-D_A_2015_CVPR_paper.html

[110] Francois Spoto, Omar Sy, Paolo Laberinti, Philippe Martimort, Valerie Fernandez, Olivier Colin, Bianca Hoersch, and Aime Meygret. 2012. Overview Of Sentinel-2. In *2012 IEEE International Geoscience and Remote Sensing Symposium*. 1707–1710. <https://doi.org/10.1109/IGARSS.2012.6351195> ISSN: 2153-7003.

[111] Gencer Sumbul, Marcela Charfuelan, Begüm Demir, and Volker Markl. 2019. Bigearthnet: A Large-Scale Benchmark Archive for Remote Sensing Image Understanding. In *IGARSS 2019 - 2019 IEEE International Geoscience and Remote Sensing Symposium*. 5901–5904. <https://doi.org/10.1109/IGARSS.2019.8900532> ISSN: 2153-7003.

[112] Xian Sun, Peijin Wang, Wanxuan Lu, Zicong Zhu, Xiaonan Lu, Qibin He, Junxi Li, Xuee Rong, Zhujun Yang, Hao Chang, Qinglin He, Guang Yang, Ruiping Wang, Jiwen Lu, and Kun Fu. 2023. RingMo: A Remote Sensing Foundation Model With Masked Image Modeling. *IEEE Transactions on Geoscience and Remote Sensing* 61 (2023), 1–22. <https://doi.org/10.1109/TGRS.2022.3194732> Conference Name: IEEE Transactions on Geoscience and Remote Sensing.

[113] K. Tachi, K. Arai, and Y. Sato. 1989. Advanced microwave scanning radiometer (AMSR): requirements and preliminary design study. *IEEE Transactions on Geoscience and Remote Sensing* 27, 2 (March 1989), 177–183. <https://doi.org/10.1109/36.20296> Conference Name: IEEE Transactions on Geoscience and Remote Sensing.

[114] Matthew Tancik, Pratul P. Srinivasan, Ben Mildenhall, Sara Fridovich-Keil, Nithin Raghavan, Utkarsh Singh, Ravi Ramamoorthi, Jonathan T. Barron, and Ren Ng. 2020. Fourier Features Let Networks Learn High Frequency Functions in Low Dimensional Domains. <http://arxiv.org/abs/2006.10739> arXiv:2006.10739 [cs].

[115] Maofeng Tang, Andrei Cozma, Konstantinos Georgiou, and Hairong Qi. 2024. Cross-Scale MAE: A Tale of Multi-Scale Exploitation in Remote Sensing. <https://doi.org/10.48550/arXiv.2401.15855> arXiv:2401.15855 [cs].

[116] Alan A. Thompson*. 2015. Overview of the RADARSAT Constellation Mission. *Canadian Journal of Remote Sensing* 41, 5 (Sept. 2015), 401–407. <https://doi.org/10.1080/07038992.2015.1104633> Publisher: Canadian Aeronautics and Space Institute _eprint: <https://doi.org/10.1080/07038992.2015.1104633>.

[117] Ramon Torres, Paul Snoeij, Dirk Geudtner, David Bibby, Malcolm Davidson, Evert Attema, Pierre Potin, Björn Rommen, Nicolas Flouri, Mike Brown, Ignacio Navas Traver, Patrick Deghaye, Berthyl Duesmann, Betlem Rosich, Nuno Miranda, Claudio Bruno, Michelangelo L'Abbate, Renato Croci, Andrea Pietropaolo, Markus Huchler, and Friedhelm Rostan. 2012. GMES Sentinel-1 mission. *Remote Sensing of Environment* 120 (May 2012), 9–24. <https://doi.org/10.1016/j.rse.2011.05.028>

[118] Gabriel Tseng, Ruben Cartuyvels, Ivan Zvonkov, Mirali Purohit, David Rolnick, and Hannah Kerner. 2024. Lightweight, Pre-trained Transformers for Remote Sensing Timeseries. <https://doi.org/10.48550/arXiv.2304.14065> arXiv:2304.14065 [cs].

[119] Arsenios Tsokas, Maciej Rysz, Panos M. Pardalos, and Kathleen Dipple. 2022. SAR data applications in earth observation: An overview. *Expert Systems with Applications* 205 (Nov. 2022), 117342. <https://doi.org/10.1016/j.eswa.2022.117342>

[120] Grant Van Horn, Oisin Mac Aodha, Yang Song, Yin Cui, Chen Sun, Alex Shepard, Hartwig Adam, Pietro Perona, and Serge Belongie. 2018. The INaturalist Species Classification and Detection Dataset. 8769–8778. https://openaccess.thecvf.com/content_cvpr_2018/html/Van_Horn_The_INaturalist_Species_CVPR_2018_paper.html

[121] Di Wang, Qiming Zhang, Yafei Xu, Jing Zhang, Bo Du, Dacheng Tao, and Liangpei Zhang. 2023. Advancing Plain Vision Transformer Toward Remote Sensing Foundation Model. *IEEE Transactions on Geoscience and Remote Sensing* 61 (2023), 1–15. <https://doi.org/10.1109/TGRS.2022.3222818> Conference Name: IEEE Transactions on Geoscience and Remote Sensing.

[122] Qunming Wang, Wenzhong Shi, Zhongbin Li, and Peter M. Atkinson. 2016. Fusion of Sentinel-2 images. *Remote Sensing of Environment* 187 (Dec. 2016), 241–252. <https://doi.org/10.1016/j.rse.2016.10.030>

[123] Yi Wang, Conrad M. Albrecht, Nassim Ait Ali Braham, Chenying Liu, Zhitong Xiong, and Xiao Xiang Zhu. 2024. Decoupling Common and Unique Representations for Multimodal Self-supervised Learning. <https://doi.org/10.48550/arXiv.2309.05300> arXiv:2309.05300 [cs].

[124] Yi Wang, Conrad M. Albrecht, Nassim Ait Ali Braham, Lichao Mou, and Xiao Xiang Zhu. 2022. Self-Supervised Learning in Remote Sensing: A review. *IEEE Geoscience and Remote Sensing Magazine* 10, 4 (Dec. 2022), 213–247. <https://doi.org/10.1109/MGRS.2022.3198244> Conference Name: IEEE Geoscience and Remote Sensing Magazine.

[125] Yi Wang, Conrad M Albrecht, and Xiao Xiang Zhu. 2022. Self-Supervised Vision Transformers for Joint SAR-Optical Representation Learning. In *IGARSS 2022 - 2022 IEEE International Geoscience and Remote Sensing Symposium*. 139–142. <https://doi.org/10.1109/IGARSS46834.2022.9883983> ISSN: 2153-7003.

[126] Yi Wang, Nassim Ait Ali Braham, Zhitong Xiong, Chenying Liu, Conrad M. Albrecht, and Xiao Xiang Zhu. 2023. SSL4EO-S12: A Large-Scale Multi-Modal, Multi-Temporal Dataset for Self-Supervised Learning in Earth Observation. <https://doi.org/10.48550/arXiv.2211.07044> arXiv:2211.07044.

[127] Yi Wang, Hugo Hernández Hernández, Conrad M. Albrecht, and Xiao Xiang Zhu. 2023. Feature Guided Masked Autoencoder for Self-supervised Learning in Remote Sensing. <https://doi.org/10.48550/arXiv.2310.18653> arXiv:2310.18653 [cs].

[128] Rolf Werninghaus and Stefan Buckreuss. 2010. The TerraSAR-X Mission and System Design. *IEEE Transactions on Geoscience and Remote Sensing* 48, 2 (Feb. 2010), 606–614. <https://doi.org/10.1109/TGRS.2009.2031062>

[129] Zhiyu Wu, Xiaokang Chen, Zizheng Pan, Xingchao Liu, Wen Liu, Damai Dai, Huazuo Gao, Yiyang Ma, Chengyue Wu, Bingxuan Wang, Zhenda Xie, Yu Wu, Kai Hu, Jiawei Wang, Yaofeng Sun, Yukun Li, Yishi Piao, Kang Guan, Aixin Liu, Xin Xie, Yuxiang You, Kai Dong, Xingkai Yu, Haowei Zhang, Liang Zhao, Yisong Wang, and Chong Ruan. 2024. DeepSeek-VL2: Mixture-of-Experts Vision-Language Models for Advanced Multimodal

Understanding. <https://doi.org/10.48550/arXiv.2412.10302> arXiv:2412.10302 [cs].

[130] Michael A. Wulder, David P. Roy, Volker C. Radeloff, Thomas R. Loveland, Martha C. Anderson, David M. Johnson, Sean Healey, Zhe Zhu, Theodore A. Scambos, Nima Pahlevan, Matthew Hansen, Noel Gorelick, Christopher J. Crawford, Jeffrey G. Masek, Txomin Hermosilla, Joanne C. White, Alan S. Belward, Crystal Schaaf, Curtis E. Woodcock, Justin L. Huntington, Leo Lymburner, Patrick Hostert, Feng Gao, Alexei Lyapustin, Jean-Francois Pekel, Peter Strobl, and Bruce D. Cook. 2022. Fifty years of Landsat science and impacts. *Remote Sensing of Environment* 280 (Oct. 2022), 113195. <https://doi.org/10.1016/j.rse.2022.113195>

[131] Zhenda Xie, Zheng Zhang, Yue Cao, Yutong Lin, Jianmin Bao, Zhuliang Yao, Qi Dai, and Han Hu. 2022. SimMIM: A Simple Framework for Masked Image Modeling. 9653–9663. https://openaccess.thecvf.com/content/CVPR2022/html/Xie_SimMIM_A_Simple_Framework_for_Masked_Image_Modeling_CVPR_2022_paper.html

[132] Zhenda Xie, Zheng Zhang, Yue Cao, Yutong Lin, Yixuan Wei, Qi Dai, and Han Hu. 2023. On Data Scaling in Masked Image Modeling. 10365–10374. https://openaccess.thecvf.com/content/CVPR2023/html/Xie_On_Data_Scaling_in_Masked_Image_Modeling_CVPR_2023_paper.html

[133] Zhitong Xiong, Yi Wang, Fahong Zhang, Adam J. Stewart, Joelle Hanna, Damian Borth, Ioannis Papoutsis, Bertrand Le Saux, Gustau Camps-Valls, and Xiao Xiang Zhu. 2024. Neural Plasticity-Inspired Multimodal Foundation Model for Earth Observation. <https://doi.org/10.48550/arXiv.2403.15356> [cs].

[134] Dejia Xu, Peihao Wang, Yifan Jiang, Zhiwen Fan, and Zhangyang Wang. 2022. Signal Processing for Implicit Neural Representations. *Advances in Neural Information Processing Systems* 35 (Dec. 2022), 13404–13418. https://proceedings.neurips.cc/paper_files/paper/2022/hash/575c450013d0e99e4b0ecf82bd1afaa4-Abstract-Conference.html

[135] Çağatay Yıldız, Nishaanth Kanna Ravichandran, Nitin Sharma, Matthias Bethge, and Beyza Ermis. 2025. Investigating Continual Pretraining in Large Language Models: Insights and Implications. <https://doi.org/10.48550/arXiv.2402.17400> arXiv:2402.17400 [cs].

[136] Jure Zbontar, Li Jing, Ishan Misra, Yann LeCun, and Stephane Deny. 2021. Barlow Twins: Self-Supervised Learning via Redundancy Reduction. In *Proceedings of the 38th International Conference on Machine Learning*. PMLR, 12310–12320. <https://proceedings.mlr.press/v139/zbontar21a.html> ISSN: 2640-3498.

[137] Qiming Zhang, Yufei Xu, Jing Zhang, and Dacheng Tao. 2022. VSA: Learning Varied-Size Window Attention in Vision Transformers. In *Computer Vision – ECCV 2022*. Shai Avidan, Gabriel Brostow, Moustapha Cissé, Giovanni Maria Farinella, and Tal Hassner (Eds.). Springer Nature Switzerland, Cham, 466–483. https://doi.org/10.1007/978-3-031-19806-9_27

[138] Weijia Zhang, Jindong Han, Zhao Xu, Hang Ni, Hao Liu, and Hui Xiong. 2024. Urban Foundation Models: A Survey. In *Proceedings of the 30th ACM SIGKDD Conference on Knowledge Discovery and Data Mining (KDD '24)*. Association for Computing Machinery, New York, NY, USA, 6633–6643. <https://doi.org/10.1145/3637528.3671453>

[139] Lijun Zhao, Ping Tang, and Lianzhi Huo. 2016. Feature significance-based multibag-of-visual-words model for remote sensing image scene classification. *Journal of Applied Remote Sensing* 10, 3 (July 2016), 035004. <https://doi.org/10.1117/1.JRS.10.035004> Publisher: SPIE.

[140] Jinghao Zhou, Chen Wei, Huiyu Wang, Wei Shen, Cihang Xie, Alan Yuille, and Tao Kong. 2022. iBOT: Image BERT Pre-Training with Online Tokenizer. <https://doi.org/10.48550/arXiv.2111.07832> arXiv:2111.07832 [cs].

[141] Yue Zhou, Litong Feng, Yiping Ke, Xue Jiang, Junchi Yan, Xue Yang, and Wayne Zhang. 2024. Towards Vision-Language Geo-Foundation Model: A Survey. <https://doi.org/10.48550/arXiv.2406.09385> arXiv:2406.09385 [cs].

[142] Xiao Xiang Zhu, Jingliang Hu, Chunping Qiu, Yilei Shi, Jian Kang, Lichao Mou, Hossein Bagheri, Matthias Häberle, Yuansheng Hua, Rong Huang, Lloyd Hughes, Hao Li, Yao Sun, Guichen Zhang, Shiyao Han, Michael Schmitt, and Yuan Yuan Wang. 2019. So2Sat LCZ42: A Benchmark Dataset for Global Local Climate Zones Classification. <https://doi.org/10.48550/arXiv.1912.12171> arXiv:1912.12171 [cs].

[143] Xiao Xiang Zhu, Zhitong Xiong, Yi Wang, Adam J. Stewart, Konrad Heidler, Yuan Yuan Wang, Zhenghang Yuan, Thomas Dujardin, Qingsong Xu, and Yilei Shi. 2024. On the Foundations of Earth and Climate Foundation Models. <http://arxiv.org/abs/2405.04285> arXiv:2405.04285 [cs, eess].

Received 16 April 2025; revised 23 October 2025